ChemistrySelect

Review
doi.org/10.1002/slct.202404345

Chemistry Europe
European Chemical Societies Publishing

www.chemistryselect.org

Applications of Graphene Derivatives in All-Solid-State Supercapacitors

Edwin T. Mombeshora,*[a] Edigar Muchuweni,[b] and Hamed Hashemi[a]

The recent progression in electronics and humankind's increased dependence on electronic gadgets have significantly impacted energy supply and demand metrics. In the past, batteries have been able to meet these demands adequately. However, their low power density (P_s) has inspired alternative energy storage advancements that can foster a transition to net-carbon-zero via renewables. Supercapacitor (SC) innovations, such as the recent emergence of solid-state supercapacitors (SSCs), have gained tremendous attention owing to their mechanical robustness, safety, possible flexibility, long cycle life, portability, prospective high P_s, and suitability for advanced energy technologies. Complimentary to the affordable and lightweight material design requirements is the enormous potential of the graphene family in SSCs owing to facile synthesis advantages, easy scalability and, processing high electrical conductivity, low costs, and mechanical robustness among others. Therefore, the review highlights the recent efforts to advance SSCs with the graphene family in electrodes and electrolytes. The work discusses SC basic concepts and main characterization techniques, and applications of the graphene family in both electrolytes and electrodes of SSCs. Finally, the merits, demerits and prospects of incorporating graphene derivatives to advance SSC performance and sustainability are outlined. Key research directions, including machine learning, are also recommended from the reviewed studies.

1. Introduction

The energy supply and demand dynamics compel robust developmental strategies in the energy storage sectors when portability, cleanliness and efficacy are considered. For example, the Internet of Everything has escalated data and power management needs.[1] Also, the drive towards a net-carbon-zero economy requires raising dependence on renewables to alleviate environmental hazards and unforeseen health complications. Dealing with intermittent glitches of most renewable energy resources and achieving sustainability requires effective energy storage facilities. Owing to their applicability in wearable devices, active radio frequency, artificial skins, and intelligent electronics,[2,3] rechargeable batteries and supercapacitors (SCs, Figure 1a) are the most common portable energy storage systems. While sustainability aspects of batteries and SCs could be addressed by improving their lifespan, thus, lowering the cost of maintenance,[3] the key to achieving higher energy storage capabilities could be hinged on the choice of materials for these devices.

Carbon-based materials, such as porous carbon,[4,5] carbon nanotubes,[6,7] nanofibers,[8] graphene,[9,10] nanocellulose,[11] and graphene derivatives[12,13]; that can be derived from biomass have shown positive traits as electrodes applicable in flexible SCs. For example, Li et al.[14] fabricated flexible polyaniline (PANI)-carbon nanotube (CNT)-reduced graphene oxide (RGO)-based solid-state SCs (SSCs) with coulombic efficiency of ~98% and specific capacitance (C_s) retention of 97% after 2000-fold bending cycles (0 – 180°). Biomass is a renewable resource, thus, reliance on biomass for deriving electrode materials has a positive impact on device costs and sustainability. Interestingly, graphene derivatives for SCs have also been derived from waste materials from spent batteries.[15] This is an important realization as far as circulatory goals are concerned. Henceforth, the material of focus in this review is graphene and associated derivatives (graphene family) as they are key in environmental sustainability through pollution mitigation.

Graphene is the basic building block of carbonaceous materials, and these comprise sp^2 C–C forming a *2D* honeycomb framework with a surface area, band gap, and electrical conductivity of 2630 $m^2\ g^{-1}$, 0 eV, and ~6×10^5 S m^{-1}, respectively.[16–20] Graphene derivatives, mainly graphene oxide (GO, area: 2600 $m^2\ g^{-1}$, band gap: 2 – 4 eV, and electrical conductivity: ~6×10^{-6} S m^{-1})[19] and RGO (area: ~500 – 800 $m^2\ g^{-1}$, tunable band gap: 0.2 – 2 eV, and electrical conductivity: ~5×10^{2} - 10^5 S m^{-1}),[19] retain the graphene backbone but with non-stochiometric oxygen moieties, primarily hydroxyl and epoxides, located at the basal plane and edges, respectively.[17] The oxygen moieties distinguish graphene derivatives from the intrinsic properties of graphene. Readers are referred to a comprehensive review[17] for a more detailed discussion on graphene derivatives. The factors that become important in graphene derivatives include heteroatom content, species, locations and distribution. These

[a] Dr. E. T. Mombeshora, Dr. H. Hashemi
School of Chemical and Metallurgical Engineering, University of the Witwatersrand, WITS 2050, Johannesburg, South Africa
E-mail: edwin.mombeshora@wits.ac.za

[b] Dr. E. Muchuweni
Department of Engineering and Physics, Bindura University of Science Education, Bindura, Zimbabwe

factors govern both feasible chemical modifications, that is, derivatization and nature of interactions in composites, and inherit properties of the graphene derivatives, which ultimately influence the performance of SCs.

In retrospection, batteries, which are more commonly used as energy storage devices, largely rely on redox flow batteries, Pb-acid and Li-ion technologies.[21,22] Each of these technologies has associated drawbacks to sustainability if their use is continued in high volumes. For instance, the cost of Li-ion batteries is rising due to Li scarcity. Furthermore, these batteries are restricted to ambient temperatures to prevent deterioration, and they are highly flammable and explosive. On the other hand, Pb-acid batteries have consequential hazardous effects on the environment. In contrast, SCs offer several advantages and are expected to reach a global market of 8.3 Billion USD by 2025.[23] A basic SC assembly consists of two electrodes, a separator and a sandwiched electrolyte (Figure 1). Using solid-based electrolytes instead of the traditional liquid is a further advancement that addresses sustainability issues of SC technology. These devices are typically known as all-solid-state supercapacitors (ASSCs/SSCs), in which a solid electrolyte is sandwiched between two electrodes (Figure 1b). Therefore, this work critically discusses the advances and challenges associated with using graphene and graphene derivatives in SSCs at the device level. The difference between the device and electrode level of SCs is in their two and three-electrode systems, respectively, dependence in characterizations. The three-electrode system used to characterize an electrode comprises the working, the reference, and the counter electrodes. One of the thrusts of the review is to highlight current shortfalls, such as ion depletions, mechanical issues, operational stability and short-term stability on conventional SCs. The review also seeks to initiate new pathways by using graphene derivatives in SSCs as electrodes and electrolytes that facilitate further modifications for addressing current shortfalls. The recent merits of graphene derivatives as additives of electrolytes and electrodes for SCs include electrical conductivity boost, lightweight, remarkable flexibility, low costs emanating from abundant sources and facile synthesis methods. Hence, the review also signposted the prospects of incorporating machine learning (ML) for SSC designing and graphene derivatives into SSCs as electrodes to potentially improve morphological properties, mechanical stability, cycle stability, capacitive properties, energy and power densities.

The major setback of SSCs is their inferior performance in terms of energy density (E_s), C_s, and P_s due to lower ion migration rates when compared to conventional liquid-based SCs.[26] On the other hand, conventional SCs, which are liquid-based, are linked with easily wettable electrodes and facile ion transport,[27] thus, performing better than SSCs. Conventional SCs are normally in bulky and rigid sandwich designs with

Dr. Edwin T. Mombeshora is a lecturer in physical chemistry in the Department of Chemistry and Earth Sciences at the University of Zimbabwe, Harare, Zimbabwe. He served as an international Technology Transfer fellow at Swansea University, United Kingdom (2021-2022). He is a member of the South African Chemical Institute and RSC Affiliate. His research interests are in Materials Chemistry and Nanotechnology. His recent research involvement as a visiting researcher at the School of Chemical and Metallurgical Engineering, University of the Witwatersrand, Johannesburg focused on the development of carbon-based materials for use as electrodes in supercapacitors.

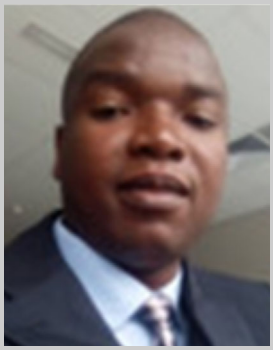

Dr. Edigar Muchuweni is a Senior Lecturer in the Department of Engineering and Physics at Bindura University of Science Education (BUSE) in Zimbabwe. His research interests include solar energy materials, nanotechnology, and materials science. In the latter, his research group works on novel nanomaterials, such as carbon nanotubes, graphene, graphene oxide, and reduced graphene oxide for several applications including energy harvesting, conversion and storage devices.

Dr. Hamed Hashemi is a senior lecturer at the University of the Witwatersrand, specializing in experimental and theoretical thermodynamics. With a focus on gas hydrates and their applications in hydrogen storage, CO_2 capture, and gas separation, Dr. Hamed Hashemi has authored numerous influential publications, including a thermodynamic model for predicting phase equilibria of clathrate hydrates and studies on refrigerant hydrate formation kinetics. In addition to research, Dr. Hamed Hashemi is dedicated to mentoring PhD students, guiding them in innovative, sustainable energy solutions that address pressing challenges in renewable energy technology and carbon reduction.

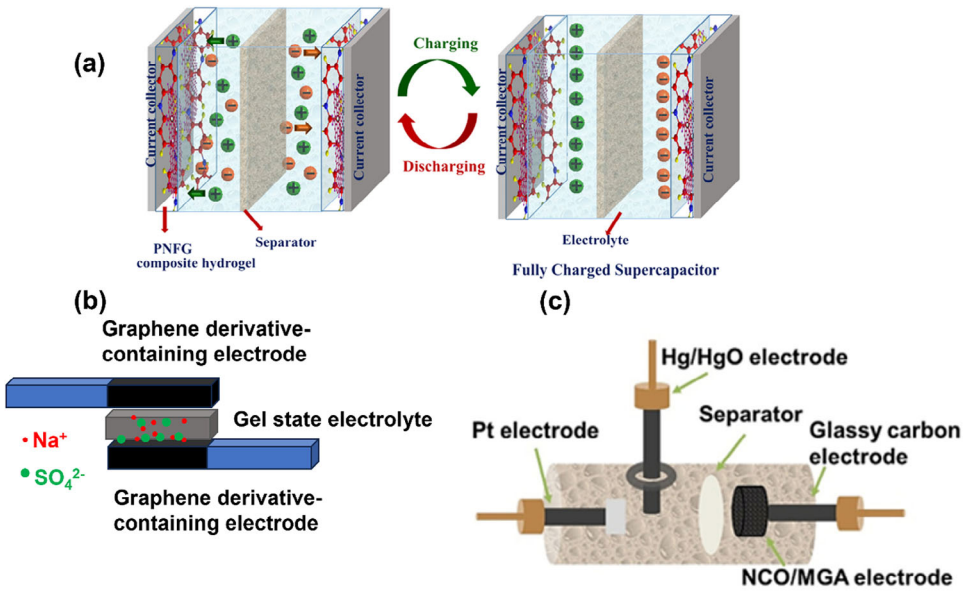

Figure 1. Illustration of (a) SCs during charging/discharging cycles, Adapted with permission, Ref. [24]. Copyright (2022), Elsevier. (b) SSCs, and (c) actual SSCs under test. Adapted with permission, Ref. [25]. Copyright (2023), Elsevier.

sealed liquid electrolytes that are fire-hazardous in cases of leakages and short-circuiting.[28] The significance of the emergence of SSCs relative to conventional designs of SCs includes being lightweight, small-sized, easy to fabricate and handle, safe, sustainable, mechanically robust, and flexible.[29–33] The elimination of binders in recent SSCs not only minimizes dead weight but also cuts down associated costs. Furthermore, SSCs solve the problems of non-elasticity and electrolyte leakages of conventional SCs. Hence, SSCs are relatively more environmentally benign than the conventional SCs. The possible elasticity in SSCs allows energy storage and release under physical twists and, therefore, can be integrated into wider applications without restrictions. Traits associated with development towards SSC have the potential to offer necessary support to the development of portable, small-sized and wearable electronics for a diverse of needs in the fourth industrial revolution to achieve commercialization, dependability and sustainability. Therefore, the basic concepts of SCs were discussed as a build-up to the SSC concept.

2. Supercapacitors

SCs are receiving a great research focus in electric vehicles, backup energy systems, and portable electronics due to their positive environmental impacts, long cycle lifetimes ($>10^5$ cycles), low maintenance costs, quick charge/discharge characteristics, stability over a wide electrochemical voltage window, and high-power density (P_s, with high power output ranging from 0.01 to 10 kW kg^{-1}).[2,34–38] The high P_s is driven by either near-surface or surface electrochemical processes that, in turn, improve diffusion and adsorption rates, respectively.[39] To achieve extensive applications and transfer from laboratory scale to market, the major focus for SCs is to enhance E_s, currently $\leq$ 10 W h·kg^{-1} for carbon-based materials,[40–42] while retaining high P_s.

2.1. Classification

Based on the charge storage mechanism, SCs fall into two main classes, namely electrochemical double layer capacitors (EDLCs) (Figure 1a) and pseudo supercapacitors (PSCs), that can be hybridized in some instances, that is., to function with both mechanisms in one device (hybrid SCs).[2,43,44] EDLCs store charge electrostatically on the electrode surface through adsorption, whereas in PSCs, storage is through reversible Faradaic reactions.[2,45,46] Advanced mechanistic investigations have revealed that pseudo-capacitive characteristics are possible through surface redox activities and ion insertions into channel or tunnel pathways of a crystalline framework, followed by fast redox reactions with minimum structural changes.[47–49] Electro-active surfaces, porosity and electrolyte nature are major drivers of C_s in EDLCs, alternatively for PSCs, performance largely depends on operational voltage, material type, pore size distribution, electro-active surfaces and morphology, among other factors.[37,47,50] Compared to EDLCs, PSCs have a higher theoretical capacity and poor cycle life.[51] For both EDLC and PSC types, the device can be said to be either asymmetric or symmetric. Symmetric SCs are made up of identical electrode materials, while in asymmetric SCs, electrode materials have differences mostly in structure and composition.[52,53]

The major mechanism difference between conventional SCs and SSCs is that the electric potential distribution in SSCs does not change to 0 V within the double layer near the electrodes, thus, there is an electrical potential difference beyond the double layer (Figure 2).

Readers are referred to reviews by Yongrui et al.[55] and Mombeshora et al.[35] for more details on charge storage

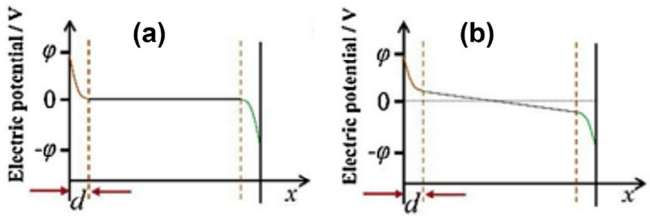

Figure 2. Illustration of difference in electric potential distribution between (a) Liquid-based SCs and (b) SSCs. Adapted with permission from Ref. [54]. Copyright (2020), Elsevier.

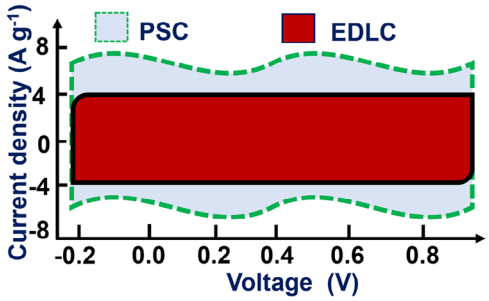

Figure 3. The illustration of the charge storage mechanism through mixed processes.

mechanisms and classifications. To know the SC types, thorough characterization is necessary.

2.2. Main Characterization Techniques

Experimental techniques such as cyclic voltammetry are useful in analyzing charge storage mechanisms using the power law (Dunn's equation)[3,56,57]:

$$i_p = av^b \quad (1)$$

where a and b are constants, i_p is the peak current measured at oxidation voltage, and v is the scan rate in mV s^{-1}, respectively. The linear form of Equation 1 allows the value of b to be obtained from the slope of $log\ i_p$ against $log\ v$. The electrochemical charge storage will be attributed to mixed, battery-like and diffusion-controlled, and surface-controlled kinetic processes (a capacitive mechanism) when values of b are $0.5 < b < 1$ (Figure 3), ~0.5 and ~1, respectively.[43] This approach is practical in determining the energy storage mechanism in composites and accounting for observed C_s changes. For example, the transformation of solvothermally synthesized RGO from capacitive to primarily battery-like and diffusion-controlled storage mechanisms in PANI-RGO was established using this technique.[56] The rationale of the transformation was porosity changes and the induction of PSC from PANI. EDLCs and PSCs display rectangular and redox peaks, respectively, on the voltammogram (brown and blue shading in Figure 3). For illustration, hybrid SCs of GO and transition metals, such as Au-Mn_3O_4//GO, have been reported to display mixed capacitive (67%) and diffusive (33%) processes ($b \sim 0.7$).[58]

On the other hand, a linear and symmetrical triangular-shaped Galvano gram from the galvanostatic charge/discharge technique indicates an ideal and fast ion response typical of EDLCs (Figure 4a).[59] However, the falsification of linearity of the galvanostatic charge/discharge curves means that the material has some pseudo-capacitive characteristics (Figure 4b),[60] and the severity of distortion is an indicator of the pseudo-capacitive contribution. It has also been reported that discharge time decreases with an increase in current density (Figure 4b). In addition, the stability aspect of SCs is determined by both CV and galvanostatic charge/discharge cycles, and in both techniques, the more the C_s retention over a large number of cycles, the better the stability characteristics.

For the Nyquist plots from impedance spectroscopy, the intercept in the real-axis of the high-frequency region and the diameter of the semicircle represents the magnitude of the equivalent series resistance (ESR) due to intrinsic factors owing to electrode nature, electrolyte ion and contact factors, and charge transfer resistance, respectively (Figure 5).[59] The major limitation of SCs is the contemporary low E_s. One key aspect of E_s is the operational voltage window, governed by the electrolyte properties. Hence, the possibility of using graphene derivatives in electrolytes for SSCs has been reviewed in the next section.

3. Applications of Graphene Derivative in Electrolytes of SSCs

The influence of electrolyte properties, such as ion mobility, size, diffusion coefficient, viscosity, conductivity and operational voltage window, on SC performance has been realized.[62,63] Expansion of the operational voltage window of electrolytes positively contributes to an increase in E_S. Liquid forms of organic

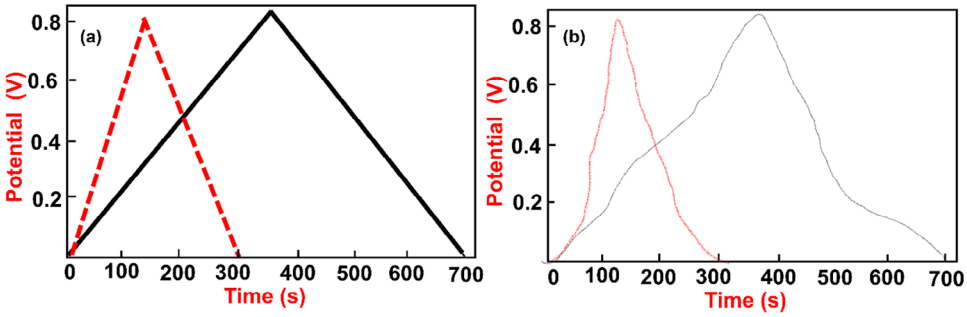

Figure 4. The illustration of (a) ideal (EDLC) and (b) distorted capacitive characteristics.

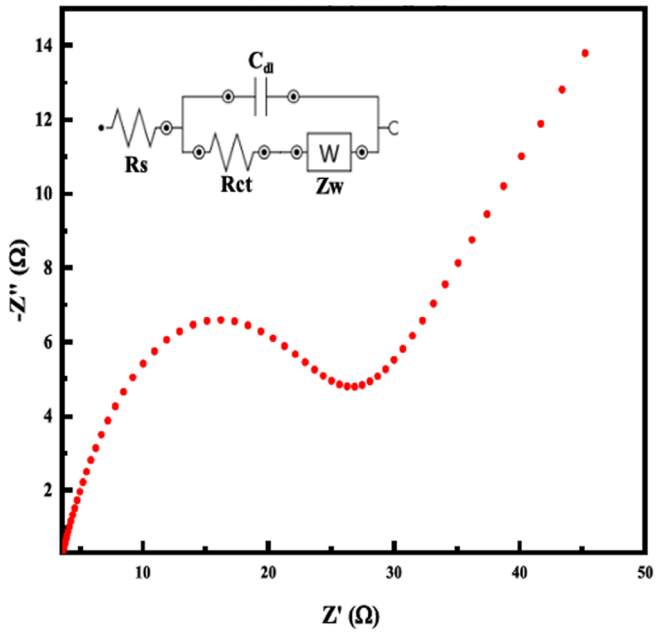

Figure 5. Illustration of a typical Nyquist plot and respective equivalent circuit. Adapted with permission, Ref. [61]. Copyright (2022), Elsevier.

compounds,[64] water-based,[65] ionic liquids,[66] and molten salts[67] are common electrolytes for SCs made up of graphene and graphene derivatives. Aqueous electrolytes are safe, environmentally friendly, affordable, and usually associated with low ESR. However, a major weakness of liquid forms is conceivable leakages, while other forms also suffer from safety concerns. Leakage-proof packaging of liquid-based SCs raises the cost of devices and minimizes flexibility and portability, and most of the liquids involved are corrosive and toxic for layman contact in case of leakages.[63,68,69] In addition, the conductivity and operational voltage window of aqueous electrolytes are ~10^2 S m^{-1} and 1 – 2.2 V, respectively.[43] Notwithstanding this, ionic and organic electrolytes, due to their wider operational voltage window, have the potential to improve the E_s of SCs, however, they are also unsafe, expensive, and have low conductivity.[43,70] Faced with all these apprehensions, researchers must actively investigate electrolyte designs that are safe, affordable, highly conductive, and functional in a broad temperature range as an alternative solution. Ionic liquid electrolytes have advanced appreciably in terms of operation in a wider temperature range due to their high thermal stability and variable temperature range tolerance.[71,72] For example, work by Sun et al.[72] was on the development of an ionic liquid-based solid-state electrolyte (PVA-Agar-GO-EMIMBF$_4$-Li_2SO_4) with self-healing capabilities of up to 95% after 5 cycles and operational in the −30–80 °C temperature range (Table 1). This demonstrates that widening the operational temperature range and flexibility enhancement, via H-bonds, of SCs is feasible through designing novel and optimized electrolyte composites.

Using solid-state electrolytes, such as ceramics and solid electrolytes confining ionic liquids (ionogels),[30,73] is a viable approach for SCs that are recommended in solving liquid electrolyte issues. These solid-state electrolytes fall into three major

Table 1. The application of graphene derivatives in electrolytes of SSCs.

OTHER electrolyte components	Electrode	C_s or specific capacity	Max conductivity (mS cm^{-1})	E_s (W h kg^{-1})	P_s (kW kg^{-1})	Stability Cycle/bent	% C_s drop	Ref
LiOAc-Agarose-GO	Activated carbon (AC)	792 mF cm^{-2} at 5 mA cm^{-2}	74	–	–	10,000	23	[34]
$LiClO_4$-Potato Starch-Chitosan-GO	$MnCoFeO_4$	288 F g^{-1} at – A g^{-1}	1	–	–	–	–	[93]
$LiClO_4$-poly(ethylene glycol-GO	–	–	50	–	–	–	–	[94]
PAM-EDTA-modified chitosan-GO	AC	52 F g^{-1} at 0.5 A g^{-1}	–	–	–	5000	5	[95]
PVA-Agar-GO-EMIMBF$_4$-Li_2SO_4	AC	130 F g^{-1} at 0.3 A g^{-1}	39	4	0.50	5000	20	[72]
PVA-PAM-GO-KOH	AC, CoNi-SP-C (positive electrode)	760.6 C g^{-1} at 1 A g^{-1}	69	56	8.29	10,000	1	[96]
PMMA-Chitosan-GO	Ag-$MnCoFeO_4$-graphene	294 F g^{-1} at – A g^{-1}	5	–	–	–	–	[97]
PVA-$AgAlO_2$-RGO	–	273 F g^{-1} at 0.5 A g^{-1}	–	13	0.15	1000	14	[90]

classes. The classes are inorganic (e.g., 2D dichalcogenide-based), redox-active, and solid polymer electrolytes.[28,74] The solid polymer type is further categorized as porous solid-, dry solid-, and gel-state polymer electrolytes.[28,75,76] Solid-state electrolytes function in both extreme cold and high temperatures.[31] An ideal solid-state electrolyte should be mechanically robust to support flexibility, highly conductive at ambient temperatures and thermally, chemically and electrochemically stable. The most applied class of solid-state electrolyte is the solid polymer. Polymer backbones in solid-state electrolytes hinder ion migration, hence, low ionic conductivity is induced due to the high crystalline nature of the material.[34,77,78] In addition, the low limit oxygen index (< 20%) makes polymer-based electrolytes highly flammable in air and the use of fire retardants (e.g., polysiloxane and phazenes) causes long-term stability and efficacy issues. To counter this, gel-state polymer electrolytes (GPE) have offered easy preparation steps, high ion conductivity with conducting polymer additives (10 S m^{-1}),[79] safe operational conditions, chemical stability, and mechanical advantages to SCs.[80] The gel is an intermediate state between solid and liquid, thus, a good compromise between the shortfalls and attributes of two phases in terms of ion migration, flexibility and robustness. The affordability aspect of gel-state electrolytes requires further clarification since the technology is still in its infancy. However, the large dependency on polymers might introduce significant costs in the new designs. Also, stability issues linked to polymers need to be carefully monitored in GPE. GPE and other solid-state electrolytes also suffer from electrode/electrolyte interfacial contact hindrances inducing high resistances.[31,81]

GPE comprise polymer frameworks, such as poly (acrylonitrile) (PAN), polyvinyl alcohol (PVA),[82] polyacrylamide (PAM),[83] and poly (methyl methacrylate) (PMMA)[84]; electrolyte salt, plasticizer (organic solvent), and usually water as the main solvent.[55,63,85] The plasticizer prevents liquid electrolyte leakage, while the polymer framework induces flexibility and stretchability traits.[55] GPE is referred to as hydrogel when water is used as a solvent. However, water limits the operational voltage and temperature windows of SSCs, and has poor electrode/electrolyte contact.[86,87] In essence, the ionic conductivity of polymer-based electrolytes can be improved by additives. For instance, adding glutaraldehyde to the PVA-H_2SO_4 achieved a conductivity of ~8 S m^{-1}.[88] However, additives that induce redox processes at the electrode/electrolyte interface may quicken the deterioration of the electrodes.[76] A crucial consideration is to ensure that the additive/polymer has strong intimacy since the conducting polymers usually have weak chemical interactions. However, GPEs are imperfect, and SSCs with only GPEs have often suffered from self-discharge issues that cause fast decay of open circuit voltage (V_{oc}) down to 50% of the charging voltage.[84] This has prompted researchers to investigate the possibility of additives to solve this problem, hence, the current work reviewed graphene derivatives as an option.

Consequently, the oxygen moieties on graphene derivative surfaces qualify it as an additive to electrolytes, as they facilitate redox processes and promote wettability on electrode surfaces.[16,36,89] The oxygen moieties aid in proton capture and H-bonding formations with polymers, which promote charge transport, thus, graphene derivatives can function as solid-state electrolyte components.[16] Theoretical studies have also hinted that GO materials are applicable as additives to polymer-based electrolytes such as agarose (a natural product of seaweed gel) to solve high flammability and low ionic conductivity (enhanced from ~0.36 to ~0.74 S m^{-1}) problems through an intimate H-bonding linkage between hydroxyl moieties of agarose and oxygen-containing groups of GO (Table 1).[34] Agarose buffers flammability via a dehydration process. However, the amount of graphene derivatives needs to be optimized. Excess amounts of graphene derivatives will cause aggregation, and ultimately charge transfer deterioration. This was demonstrated by Somesh et al.,[90] who showed that incorporating a 2 wt.% of $AgAlO_2$-RGO into PVA/$AgAlO_2$-RGO solid-state electrolyte improved C_s by ~46 fold, beyond which the performance deteriorated (Table 1). Notable impacts of graphene-based materials in electrolytes for SSCs include minimization of dead mass by avoiding concentrators, binders and additional conductive additives.[91,92] Two main classes result from the graphene derivative inclusion in gel-state electrolytes, namely, hydrogel and aerogel, owing to their different synthesis methods, that is., GO reduction in water and other solvents, respectively. Readers are referred to a detailed review of early graphene derivative-based gels reported by Zhang et al.[91] However, the present review focuses more on the period from 2022 to 2024, which was not covered in the cited review.

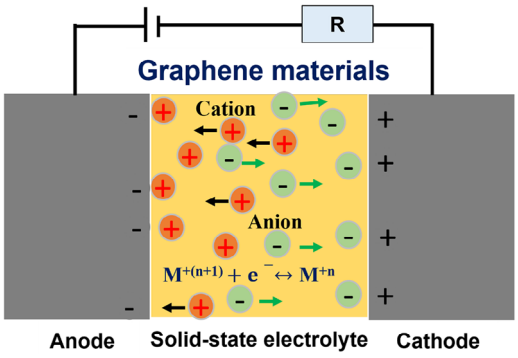

Figure 6. Illustration of the application of graphene derivatives in solid-state electrolytes.

Interestingly, in recent times, the widely applied graphene derivative in solid-state electrolytes is GO,[34,72,93–97] even though it has relatively lower conductivity than RGO (Table 1 and Figure 6). This could be because of the vast oxygen-containing functionalities that form strong H-bonds with polymers such as PVA via OH moieties. Therefore, GO is more suitable as an electron pathway because of better intimacy. Reviewed works indicate that solid-state electrolytes are commonly ternary composites in which the polymer induces the quasi-solid state features, and the cations transfer the charges between electrode surfaces (Table 1). The highly conductive LiOAc-Agarose-GO[34] and PVA-PAM-GO-KOH[95] not only have high C_s but also achieved low C_s drops after 10^4 charge/discharge cycles (Table 1). GO has also been demonstrated to positively impact a cation-based solid-state electrolyte by Lei et al.[98] (4×10^3 conductivity enhancement). This means that despite having a few reports on graphene-based solid electrolytes, the graphene derivative

additives have positive prospects in GPE, as most reviewed articles culminated in enhanced energy storage performances. Hence, more studies are needed on graphene derivative-based solid-state composites for SSCs as a future research direction.

The PVA-based electrolytes in combination with group one cations are commonly reported in SSCs involving graphene and graphene derivatives (Tables 2, 3). The main inspiration is most likely to be facile synthesis and affordability merits. Furthermore, the group one cations are combined with anions, namely SO_4^{2-} and OH^- (Tables 2, 3). However, the choices of cations, anions, and combinations to form gel-state electrolytes for SSCs seem random with no defined criteria in the literature.

Therefore, future studies should investigate the effect of cationic and anionic sizes in gel-state electrolytes using the same graphene-based electrode materials to shed more light on these critical aspects. Thus, the review also focused on the recent developments of graphene derivative-based electrodes of SSCs, among other breakthroughs.

4. Graphene Derivatives as Electrode Material for SSCs

Based on the Equation 2:

$$E_s = \frac{1}{2} C_s V^2 \quad (2)$$

improving C_s directly enhances E_s. In addition, C_s is greatly influenced by the intrinsic factors of the electrode.[59,99,100] This is the reason for the contemporary major focus on SC electrode materials. Therefore, this has led to a majority of reports being at electrode levels and this could be an incomplete story to gauge the real progress attained to date. The current work was solely at the device level for two reasons. First, it is easier, if not the only possibility to characterize graphene derivatives for SSCs. Second and most importantly, the motivation was to establish the actual device performance of the materials. Recently, some literature has given characterization at both levels and this is a positive shift of research directions. Modifying the physicochemical properties of the electrode material will, in turn, alter C_s and ultimately E_s.[101,102] For instance, since electrical potential is generated at the electrode/electrolyte interface by the electrons being deficient and excess in the conduction band,[53] tuning the electronic structure to improve charge transfer of the electrode material induces changes to E_s. Understanding the charge storage mechanisms in novel materials is a fundamental research direction towards designing advanced SSCs. For example, fabrication of hybrid capacitors is only possible when their mode of charge storage is known, and the approach aids the balancing of E_s with P_s in devices. The materials with EDLC and PSC characteristics will contribute to P_s (owing to high electro-active surfaces, electrochemical stability and electronic conductivity) and E_s enhancement, respectively.[36,39,53] The energy stored in both types of SCs is proportional to the number of active materials.[47] For example, PSC materials such as transition metals are good electrode materials, however, their nature often limits electro-active sites and, hence, presents a hindrance to electron/ion transfer and long-term stability in ECs.[2,101,103] Readers are referred to a review by Kumar et al.[103] for an in-depth review of metal-graphene derivative materials for SCs.

Therefore, the limitations in PSC materials have triggered the inclusion of EDLC materials such as graphene derivatives in representative electrodes (Tables 2, 3). Bahaa et al.[104] fabricated a $CoSe_2$/PVA-KOH/Fe-TiN-N-doped graphene SSC via a hydrothermal method on Ni foam. Their device achieved an expanded operational voltage window of $CoSe_2$ from 0.8 to 1.8 V (Table 3). Zhang et al.,[105] connected three Co_3O_4 nanorods/PVA-KOH/RGO SSCs, made by pressing the active material at 6 MPa pressure onto Ni foam, in series raised the operational voltage window from 1.4 to 4.4 V at 5 A m^{-2} (Table 3). Similarly, Vandana et al.[106] improved the operational voltage window from 0.74 to 2.44 V using SnO_2 quantum dots (QDs)-GO-PPY bladed onto titanium foil (Table 2). This illustrates another strategy to expand E_s of SSCs that has been achieved in recent studies in both symmetric and asymmetric SSCs (Tables 2, 3). The highlighted works suggest that future research drivers must consider understanding the energy storage mechanisms in electrode materials as the basic step needed for novel hybrid SSC designs. Therefore, it is clear that the compositing of graphene derivatives with pseudocapacitive materials is promising in expanding the operational voltage window of SSCs and, in turn, positively impacts E_s. This is emphasized by SSC symmetric devices reviewed in this work. For example, pristine graphene and RGO achieved lower E_s values when compared to their composite counterparts (Table 2). In addition, the effects of covalency of bonding between graphene derivatives and electrolyte ions on performance[36] are underexplored, despite possibly being a critical factor. The covalency of bonding between components needs dedicated investigations as a future research direction.

Pristine graphene, with a theoretical C_s of 550 F g^{-1},[107] has high agglomeration rates due to $\pi-\pi$ stacking, thus, inducing poor electrolyte penetration, contact resistance and low C_s values.[108] The laser engraving technique has been reported as a suitable strategy to avoid weaknesses of pristine graphene in SSCs. For example, Zhao et al.[109] directly used a laser to engrave conductive graphene-assembled films to form SSCs with low ESR (4.1 Ω) and long-term stability (~98% C_s retention after $> 2.5 \times 10^4$ cycles). Additionally, Jagdale et al.[110] also designed a flexible SSC on micropatterned laser-scribed graphene, comprising of 3.5 nm $Co(OH)_2$, nanosheets with high E_s (22 mW h cm^{-3}), and P_s (6.8 W cm^{-3}), along with outstanding stability (~96% C_s retention after 2×10^4 cycles). These two studies signify high C_s retentions when laser engraving is used in SSC fabrication, thus, it is a lucrative way to enhance the lifespan of future devices. On an industrial scale, laser engraving is easy to manage during fabrication and it ensures good reproducibility. Another suitable technique is the 3D printing of SSCs using graphene ink at low temperatures such as the 40 °C reported by Kumar et al.[111] that achieved a C_s of 137 F g^{-1} at 0.5 A g^{-1} (Table 2). Furthermore, Raihan et al.[112] used printed graphene for fabricating flexible PVA-H_3PO_4-based SSCs that attained C_s of ~377 mF cm^{-3} at 0.25 μA and C_s retention of ~100% after 10^4 cycles. Also, Han et al.[113] reported a mechanically strong (~52×10^3 N m kg^{-1}) and highly conductive (119 S m^{-1}) *3D*

Review
doi.org/10.1002/slct.202404345

Chemistry Europe
European Chemical Societies Publishing

Table 2. The application of graphene derivatives as an active material of symmetric SSCs.

Active material	Electrolyte	C_s or specific capacity	E_s	P_s	Stability		Ref
					Cycle (10^4)	$\%C_s$ drop	
Graphene application							
Graphene	PVA-table sea salt	32 F g^{-1} at 0.25 A g^{-1}	6 W h kg^{-1}	600 W kg^{-1}	0.8	13	[119]
Graphene	PVA-Na_2SO_4	238 F g^{-1} at 1 A g^{-1}	27 W h kg^{-1}	450 W kg^{-1}	0.5	4	[118]
Graphene	PVA-Na_2SO_4	137 F g^{-1} at 0.5 A g^{-1}	12 W h kg^{-1}	800 W kg^{-1}	–	–	[111]
Borophene-graphene	PVA-KOH	193 at 0.5 A g^{-1}	37 W h kg^{-1}	585 W kg^{-1}	2	19	[129]
CuSP nanosheets-Cu-graphene fiber	PVA-KOH	–	0.16 W h m^{-2}	–	0.5	5	[121]
PANI-MWCNT-graphene	PVA-K_2SO_4	423 F g^{-1} at 1 A g^{-1}	100 W h kg^{-1}	500 W kg^{-1}	0.5	21	[126]
PPY-graphene	PVA-H_2SO_4	134 F g^{-1} at 1 A g^{-1}	60 W h kg^{-1}	900 W kg^{-1}	1	16	[127]
MoSSe-graphene-graphitic petal	PVA-K_2SO_4	2520 F m^{-2} at 30 A m^{-2}	0.11 W h m^{-2}	1300 W m^{-2}	0.4	20	[108]
N-graphene	–	122 F g^{-1} at 1 A g^{-1}	17 W h kg^{-1}	16,000 W kg^{-1}	1	9	[120]
Al-CoS_2-N doped graphene	PVA-KOH	188 F g^{-1} at 1 A g^{-1}	67 W h kg^{-1}	800 W kg^{-1}	1	8	[122]
g-C_3N-N doped graphene	[EMIM][BF_4]-PVDF-KOH/ p-phenylenediamine	1410 F m^{-2} at 11 A m^{-2}	–	7 W m^{-2}	1.8	1	[128]
Nb_9VO_{25}-histidine-serine-B-graphene QDs	PVA-Li_2SO_4	263 F g^{-1} at 1 A g^{-1}	146 W h kg^{-1}	1 000 W kg^{-1}	1	8	[123]
GO application							
AC-GO-TiO_2-Zn	PVA-KOH	1492 F g^{-1} at 2.5 A g^{-1}	99 W h kg^{-1}	3570 W kg^{-1}	1	39	[131]
Chitosan-GO	Lignin hydrogel	210 F g^{-1} at 0.5 A g^{-1}	31 W h kg^{-1}	150 W kg^{-1}	1	2	[59]
Chitosan-N-GO	PVA-KOH	59 F g^{-1} at 0.25 A g^{-1}	15 W h kg^{-1}	–	0.05	9	[115]
Carbon cloth-NiAl- layered double hydroxide (LDH)-GO-NiCo-LDH	PVA-KOH	146 F g^{-1} at 1 A g^{-1}	52 W h kg^{-1}	800 W kg^{-1}	0.15	14	[132]
Au-Mn_3O_4-GO	PVA-H_2SO_4	124 F g^{-1} at 1 A g^{-1}	56 W h kg^{-1}	4500 W kg^{-1}	1	6	[58]
Co[$(CN)_6$Fe]-GO	PVA-Na_2SO_4	78 F g^{-1} at 1 A g^{-1}	46 W h kg^{-1}	2100 W kg^{-1}	1	1	[99]
PANI-GO	PVA-H_2SO_4	213 F g^{-1} at 1 A g^{-1}	20 W h kg^{-1}	400 W kg^{-1}	0.5	16	[133]
PPY-GO	PVA-H_2SO_4	–	1.14 W h m^{-2}	5.00 W m^{-2}	0.5	4	[145]
PPY-GO-MnO_2-carbon cloth	PVA-H_2SO_4	114 F g^{-1} at 0.5 A g^{-1}	23 W h kg^{-1}	4.60 W kg^{-1}	0.5	17	[149]
PPY-GO-Ni	PAM-MXene	92 F g^{-1} at 0.3 A g^{-1}	–	–	0.1	28	[157]
PPy-Ag-GO-cotton fabric	PVA-H_2SO_4	2900 F m^{-2} at 0.05 A m^{-2}	0.26 W h m^{-2}	1.02 W m^{-2}	1	9	[134]
SnO QDs-GO-PPY	PVA-KOH	786 F g^{-1} at 1 A g^{-1}	26 W h kg^{-1}	4100 W kg^{-1}	1.1	22	[106]
ZnO doped SnO_2-GO-PPy	PVA-KOH	326 F g^{-1} at 0.25 A g^{-1}	32 W h kg^{-1}	5180 W kg^{-1}	1.5	8	[146]

Review
doi.org/10.1002/slct.202404345

Chemistry Europe
European Chemical Societies Publishing

Table 2. (Continued)

Active material	Electrolyte	C_s or specific capacity	E_s	P_s	Stability Cycle (10^4)	Stability %C_s drop	Ref
RGO application							
RGO	Methyl grafted natural rubber-CF_3NaO_3S	43 F g^{-1} at 10 mV s^{-1}	2 W h kg^{-1}	440 W kg^{-1}	1	21	[155]
RGO	PVA-H_2SO_4	263 F g^{-1} at 0.5 A g^{-1}	37 W h kg^{-1}	500 W kg^{-1}	0.5	10	[158]
Carbon cloth-PANI-RGO	PVA-H_2SO_4	262 F g^{-1} at 0.5 A g^{-1}	53 W h kg^{-1}	300 W kg^{-1}	1	17	[147]
Cellulose nanofibrils-RGO	PVA-H_2SO_4	312 F m^{-2} at 30 A m^{-2}	–	–	0.5	18	[152]
Cellulose nanofiber-RGO	PVA-KOH	193 F g^{-1} at 1 A g^{-1}	5.25×10^6 W h m^{-3}	2.04×10^9 W m^{-3}	0.5	6	[150]
PPY-TEMPO-oxidized cellulose nanofiber-RGO	Cellulose nanofiber-H_2SO_4	196 F g^{-1} at 0.1 mA g^{-1}	13 W h kg^{-1}	0.20 W kg^{-1}	0.08	13	[151]
Nano cellulose-N, F-GO	PVA-KOH	117 F g^{-1} at 0.3 A g^{-1}	–	–	1	17	[153]
3D printed Co_3O_4-RGO	PVA-KOH	32 F g^{-1} at 0.5 A g^{-1}	6 W h kg^{-1}	280 W kg^{-1}	0.1	10	[113]
Co_3O_4-polydopamine-RGO	PVA-KOH	180×10^6 F m^{-3} at 0.5 A m^{-2}	12 000 W h m^{-3}	2.60×10^5 W m^{-3}	0.3	5	[148]
CuCo-LDH-RGO	PVA-KOH	45 F g^{-1} at 2 A g^{-1}	8 W h kg^{-1}	670 W kg^{-1}	0.5	21	[159]
N-Cu-metal organic framework (MOF)-RGO	PVA-Na_2SO_4	153 F g^{-1} at 0.5 A g^{-1}	31 W h kg^{-1}	0.60 W kg^{-1}	1	10	[77]
Fe^{3+}-$Ti_3C_2T_x$-S-,N-RGO	PVA-KOH	74 F g^{-1} at 1 A g^{-1}	17 W h kg^{-1}	0.66 W kg^{-1}	1	0	[46]
KCu_7S_4-RGO	PVA-KOH	79 F g^{-1} at 0.1 A g^{-1}	3 W h m^{-2}	21.60 W m^{-2}	0.5	17	[160]
Mn_3O_4-RGO	PVA-Na_2SO_4	418 F g^{-1} at 0.5 A g^{-1}	22 W h kg^{-1}	3.00 W kg^{-1}	0.5	10	[161]
MoS_2-RGO fiber fabric	PVA-H_2SO_4	9800 F m^{-2} at 10 A m^{-2}	0.69 W h m^{-2}	50 W m^{-2}	0.5	10	[135]
PAN-RGO-PPy	PVA-KOH	108 F g^{-1} at 1 A g^{-1}	15 W h kg^{-1}	0.50 W kg^{-1}	1	24	[136]
Al_2O_3-RGO-PANI- dodecylbenzene sulfonic acid (DBSA)-polylactic acid (PLA)/	PVA-H_2SO_4	173 F g^{-1} at 1 A g^{-1}	15 W h kg^{-1}	–	0.5	15	[137]
Steel-RGO-PANI-DBSA-PLA		134 F g^{-1} at 1 A g^{-1}	11 W h kg^{-1}	–	0.5	23	
Cu-RGO-PANI-DBSA-PLA		160 F g^{-1} at 1 A g^{-1}	13 W h kg^{-1}	–	0.5	19	
Oxidised carbon cloth-PANI-RGO	PVA-H_2SO_4	14,300 F m^{-2} at 10 A m^{-2}	1.18 W h m^{-2}	4.30 W m^{-2}	0.2	10	[138]
Oxidised carbon cloth-PPY-RGO	PVA-H_2SO_4	244 F g^{-1} at 0.5 A g^{-1}	34 W h kg^{-1}	0.25 W kg^{-1}	0.1	5	[139]
PEDOT-RGO-MoS_2	PVA-KCl	0.008 F g^{-1} at 0.001 A g^{-1}	0.01 W h m^{-2}	0.50 W m^{-2}	1	2	[74]
PET-RGO	PVA-H_2PO_4	212 F g^{-1} at 1 A g^{-1}	–	–	1	2	[156]
PolyIndole (PIn)-SbO_x-Ag_2O-Au-RGO	PVA-Na_2SO_4	182 F g^{-1} at 2 A g^{-1}	41 W h kg^{-1}	1.00 W kg^{-1}	1.2	18	[89]

Table 3. The application of graphene derivatives as an active material of Asymmetric SSCs.

Active Material (Anode//cathode)	Electrolyte	C_s or specific capacity	E_s	P_s	Stability Cycle (10^4)/Bent	% C_s drop	Ref
Graphene application							
Ni-Co LDH-Co_3O_4//graphene	PVA-KOH	286 F g^{-1} at 1 A g^{-1}	67 W h kg^{-1}	800 W kg^{-1}	1.05	9	[70]
Al-doped Co_9S_8-N-doped graphene//activated PANI derived carbon nanorods	PVA-KOH	134 F g^{-1} at 1 A g^{-1}	53 W h kg^{-1}	950 W kg^{-1}	1	7	[124]
Asphalt-graphene QDs-NiCo LDH//AC	PVA-KOH	360 F g^{-1} at 1 A g^{-1}	113 W h kg^{-1}	751 W kg^{-1}	0.5	29	[125]
$CoSe_2$//Fe-TiN-N-doped graphene	PVA-KOH	–	92 W h kg^{-1}	280 W kg^{-1}	1	5	[104]
$CeCoS_x$-sodium alginate-S,N co-doped graphene//AC	PVA-KOH	92 F g^{-1} at 0.5 A g^{-1}	30 W h kg^{-1}	800 W kg^{-1}	0.5	17	[10]
$CoWO_4$-$CoMn_2O_4$-N-doped graphene//AC	Filter paper-KOH	282 F g^{-1} at 0.001 A g^{-1}	0.06 W h kg^{-1}	0.60 W kg^{-1}	–	–	[61]
Ni-MnO_2-CNTs-N-graphene//CNTs-N-graphene	PVA-$LiClO_4$	90 × 10^6 F m^{-3} at 10 A m^{-2}	79 × 10^3 W h m^{-3}	–	1	9	[64]
GO application							
Co-Cr-LDH-GO//RGO	PVA-KOH	131 F g^{-1} at 0.002 A g^{-1}	47 W h kg^{-1}	1540 W kg^{-1}	1	9	[162]
Fe_3O_4-GO//$GdMnO_2$-$Ni(OH)_2$	PVA-KOH	120 F g^{-1} at 2 A g^{-1}	60 W h kg^{-1}	2330 W kg^{-1}	1	10	[163]
$Ni(OH)_2$-GO//AC	PVA-KOH	3220 F m^{-2} at 0.005 V s^{-1}	134 W h m^{-2}	0.034 W kg^{-1}	0.1	20	[164]
ZnO nanowire-GO//FTO	PVA-LiCl	7 F g^{-1} at 0.2 A g^{-1}	5.62 W kg^{-1}	–	3	0	[165]
ZnO nanowire-GO//FTO	PVA- LiCl	2200 F g^{-1} at 0.03 A g^{-1}	2 W h kg^{-1}	–	0.5	0	[117]
RGO application							
ZnO nanowire-RGO//FTO	PVA- LiCl	875 F g^{-1} at 0.03 A g^{-1}	1 W h kg^{-1}	–	0.5	30	
RGO//Ni–$Mn_3(PO_4)_2$	PVA-KOH	192 C g^{-1} at 0.6 A g^{-1}	48 W h kg^{-1}	580 W kg^{-1}	0.5	+8	[174]
$Ni_{3-x}Co_x(PO_4)_2 \cdot nH_2O$//RGO	PVA-KOH	102 F g^{-1} at 0.2 A g^{-1}	36 W h kg^{-1}	160 W kg^{-1}	0.4	16	[166]
$Co(OH)_2$-RGO//AC	PVA-KOH	154 F g^{-1} at 0.5 A g^{-1}	28 W h kg^{-1}	1750 W kg^{-1}	0.4	11	[167]
Co_3O_4 nanorods//RGO	PVA-KOH	1900 F m^{-2} at 5 A m^{-2}	1.87 W h m^{-2}	12.60 W m^{-2}	0.1	17	[105]
CoS_2-graphitic C-RGO//RGO	PVA-KOH	233 F g^{-1} at 1.5 A g^{-1}	83 W h kg^{-1}	1200 W kg^{-1}	1	13	[168]
CuO-TiO_2-RGO//AC	PVA-H_2SO_4	564 F g^{-1} at 0.001 A g^{-1}	50 W h kg^{-1}	500 W kg^{-1}	0.5	22	[169]
MnO-RGO//AC	Polyvinylidene fluoride-hexafluoro propylene	76 F g^{-1} at 0.1 A g^{-1}	195 W h kg^{-1}	270 W kg^{-1}	1	22	[175]
MXene-RGO//$NiCo_2S_4$	PVA-KOH-$K_4[Fe(CN)_6$	98 F g^{-1} at 4.5 A g^{-1}	36 W h kg^{-1}	3690 W kg^{-1}	0.4	5	[176]
N-(Nb_2C-RGO)//N-(Nb_2C-RGO)	PVA-H_2SO_4	176 F g^{-1} at 0.5 A g^{-1}	10 W h kg^{-1}	2400 W kg^{-1}	10	0	[170]
Ni–Cr LDH-GO//RGO	PVA-KOH	108 F g^{-1} at 2 A g^{-1}	39 W h kg^{-1}	1330 W kg^{-1}	1	3	[177]
Al-Co_xP-RGO//PANI-derived carbon nanorods	PVA-KOH	217 F g^{-1} at 1 A g^{-1}	77 W h kg^{-1}	1050 W kg^{-1}	1	10	[52]
Br-RGO//N-RGO	PVA- $NaClO_4$	251 F g^{-1} at 1 A g^{-1}	55 W h kg^{-1}	1250 W kg^{-1}	1	15	[11]
$CuCo_2O_4$-RGO//Ni-RGO	Polyethylene oxide-LiOTf	4390 F m^{-2} at 3 A m^{-2}	2 W h m^{-2}	2.70 W m^{-2}	0.5	5	[171]
$FeNi_2S_4$-Co_9S_8-RGO//NiFe-AC	Cellulose-KOH	1308 C g^{-1} at 1 A g^{-1}	69 W h kg^{-1}	860 W kg^{-1}	0.85	5	[140]
Ni MOFs-RGO//AC	PVA-KOH	102 F g^{-1} at 1 A g^{-1}	36 W h kg^{-1}	800 W kg^{-1}	0.1	1	[178]
$NiCo_2O_4$-$Ti_3C_2T_x$ MXene-RGO//$Ti_3C_2T_x$ MXene-RGO	PVA-KOH	87 F g^{-1} at 1 A g^{-1}	41 W h kg^{-1}	1120 W kg^{-1}	1	13	[25]
$NiMoO_4$-RGO-polypyrrole (PPy)//AC-Graphite	PVA-KOH	218 F g^{-1} at 1 A g^{-1}	44 W h kg^{-1}	600 W kg^{-1}	~70°	29	[2]
$NiWO_4$-RGO//AC	PVA-KOH	94 F g^{-1} at 5 A g^{-1}	33 W h kg^{-1}	12.37	0.5	17	[3]
Zn//B-C QDs-RGO	Gelatin $ZnSO_4$	271 F g^{-1} at 0.5 A g^{-1}	890 W h m^{-2}	96 × 10^4 W m^{-2}	1	2	[172]
Zn//N-P-RGO	Potassium polyacrylate-sodium carboxymethyl cellulose-$Zn(CH_3COO)_2$-CH_3COOK	195 F g^{-1} at 0.5 A g^{-1}	107 W h kg^{-1}	380 W kg^{-1}	0.8	13	[173]

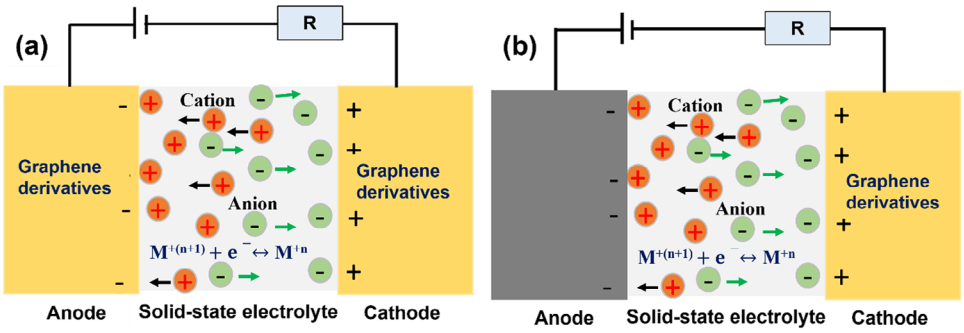

Figure 7. Illustration of graphene derivative applications as electrodes of; (a) symmetric and (b) asymmetric all-solid-state supercapacitors.

printed Co_3O_4-RGO for energy storage application (Table 2). Their reported mechanical strength of graphene derivative composites highlights the potential of compositing and *3D* printing in reinforcing the durability of SSCs as a future research direction.

Graphene derivatives as an alternative displayed high electro-active surface area, electrochemical robustness, and EDLC characteristics induced by their carbon backbone. Thus, graphene derivatives are associated with ultrafast charge/discharge traits of $<10^4$ cycles at the electrode/electrolyte interface.[2,21,114] In particular, RGO is generally known to have better mechanical strength, electro-active surface area, and electrical conductivity than GO, hence, RGO is mostly used in recent SSCs at the device level (Tables 2, 3 and Figure 7). To enhance the surface area, Mo et al.[115] reported a potassium citrate activation at 600 °C for chitosan-nitrogen-doped GO (N-GO, ~ 4 at. % N) that raised surface area by two-fold when activation temperature was raised from 500 to 600 °C and displayed an increase in EDLC contribution to C_s with scan rate (76% to 97% for 2 and 200 mV s^{-1}, Table 2). This supports the idea that a large electro-active surface area positively impacts charge storage through the EDLC mechanism. However, details about the most appropriate method for the electro-active surface area determination remain unclear in the literature. Some studies have highlighted that surface area measured utilizing nitrogen sorption analysis does not necessarily coincide with electro-active surface area.[116] This is rationalized by the fact that the method utilizes the Brunauer–Emmett–Teller (BET) equation, which gives the total surface area that is not certainly available as electro-active surfaces for charge storage.[6] This is logical when electrolyte ionic sizes are considered against the size of the N_2 molecules used in the BET equation.

It is essential to note that the ultimate energy storage performance is governed by synergistic factors of graphene derivatives and other components in the electrode material, counter electrode, and electrolyte. Therefore, a more accurate comparison of graphene derivatives requires pristine materials and similar experimental parameters. The development of standardized testing protocols for materials is needed shortly to revolutionize the entry of graphene derivatives in commercial markets. A critical analysis of recent works on symmetric SSCs reviewed (Table 2) assumed that all comparison constraints are negligible and considered only champion performances of SSCs with graphene, GO, and RGO for respective electrolytes. Analysis of C_s suggests that RGO-based SSC electrodes had superior values in both PVA-Na_2SO_4 and PVA-H_2SO_4 electrolytes. The C_s of graphene- and GO-based electrodes were second in PVA-Na_2SO_4 and PVA-H_2SO_4 electrolytes, respectively. Remarkably, the E_s in the same electrolytes were within similar ranges for GO and RGO but better than that of graphene. For P_s, GO electrodes were highest in the two electrolytes followed by those of graphene. GO-based electrodes displayed champion C_s, E_s, and P_s in PVA-KOH while RGO had the lowest values in C_s and E_s. Despite the expected norm of having RGO performing better than GO in SSCs, Altaf et al.[117] reported an opposite trend in their photo-assisted SSCs fabricated by the spin coating method (Table 3). They rationalized their results through paramagnetic resonance spectroscopy and V_{oc} analysis in dark and UV light illumination in which they deduced a higher leap in V_{oc} with GO material that took over 2 h to relax. This highlights how photo-assisted SSCs containing graphene derivatives have the potential to bring new perspectives to energy storage. Therefore, future research approaches need thorough characterization and optimization steps.

To circumvent the current shortfalls of SSCs, various electrode advances have been made with graphene derivatives (Tables 2, 3). Despite a few recent reports on graphene application in symmetric SSCs (Table 2, Figure 7a), their utilization has achieved appreciable C_s. For example, the *3D* printing approach to SSCs using pristine graphene[111] and the same electrolyte has shown that these devices were inferior to their blade-coated[118] and solution-casted[119] counterparts in both C_s and E_s (Table 2). This highlights how an SSC fabrication method can impact performance owing to electrode qualities. Furthermore, the outcomes could also have been influenced by the graphene material synthesis method which were microwave-assisted pyrolysis and solution casting in the counterparts, respectively, and unspecified in the 3D printed study. Reported N-doping of graphene displayed a significant improvement in P_s (16 kW kg^{-1}) though the C_s improvement was negligible.[120] This could be due to faster redox activities induced by nitrogen moieties. Another way to tailor graphene is by decorating its carbon backbone through compositing with transition metals[64,104,108,121–125] and conducting polymers[126,127] (Tables 2, 3). For illustration, *2D* MoSSe sheets were composited with graphene-graphitic petals using the hydrothermal method to enhance charge transport pathways for energy storage through the PSC mechanism and intimate chemical linkages.[108] The R_{ct} of the composites was smaller (2.7 Ω) compared to that of *2D* MoSSe sheets (195 Ω) and SSC displayed almost 100% Columbic efficiency after 4000

cycles. A binder-free PANI-MWCNT-graphene-graphite-based SSC attained 424 F g^{-1} at 1 A g^{-1} in PVA-H_2SO_4 electrolyte, which was sufficient to power 6 light-emitting diodes (LEDs) of 1.8 V.[126] This was ascribed to improved wettability (contact angle decreased to ~29° from ~58°) and ~2-fold increment in surface area. The study is a demonstration of the possibility of eliminating binders in SSCs. Two highly flexible PPy-graphene SSC devices, synthesized by the hydrothermal method and connected in series, with P_s of 900 W kg^{-1} in PVA-H_2SO_4 electrolyte were able to light up an LED of 2 V while bent at angles of 90° and 135°.[127] These studies are feasible examples that highlight the practical significance of graphene derivatives in SSCs. Al-CoS_2-N doped graphene SSC achieved a 92% C_s retention after 10^4 cycles owing to a decline of R_s (from 17.4 to 1.02 Ω) and P_s of 800 W kg^{-1} in PVA-KOH electrolyte.[122]

Heteroatom doping and other surface functionalities introduce pseudo-capacitance traits.[11,24,56,61,123,128,129] Hence, improve energy storage capabilities, while lowering the kinetics due to redox reactions on particular moieties.[2,3,114] N-doping positively tailored the electronic properties of graphene derivatives (Fermi level), consequently improving C_s.[21,36,130] From the compositing perspective, additives to graphene derivatives improve electroactive surface area (improve porosity), and modulate crystallinity, thus, improving lifespan and performance by inducing *2D* conducting channels in the electrode.[3,48,130–139] For example, performance (E_s: ~44 W h kg^{-1} and C_s: ~218 F g^{-1}) and lifespan were enhanced through a ternary composite of PANI, N-GO and sulfur-doped GO (S-GO) with no capacity deterioration after 1500 cycles (> 100% of initial the C_s).[21] In another study, evenly dispersed nanoscale Fe_2O_3 particles on the highly conductive $Ti_3C_2T_x$/S, N-RGO composite maintained layer spacing between nanosheets, which facilitated a larger electroactive area and shortened the ion diffusion path length, enabling the SSC to operate effectively under extreme conditions of −20–60 °C with 100% C_s retention after 10^4 cycles and P_s of 0.66 W kg^{-1} (Table 2).[46] Moreover, the $FeNi_2S_4$-Co_9S_8-RGO composite displayed an 84% capacity retention when the current density was raised from 1 to 36 A g^{-1} (Table 3).[140] Also, the Co[$(CN)_6$Fe]-GO composite achieved a high-rate capability in flexible SSCs when current density was raised from 1 to 15 A g^{-1} (71% C_s retention) owing to large electro-active surfaces induced by Co[$(CN)_6$Fe] uniform dispersion, conductivity attributes from GO/Co[$(CN)_6$Fe] intimacy and GO volume expansion buffering (flexibility and stability).[99] These studies are a testament to the positive attributes that can be achieved by compositing graphene derivatives with transition metals to improve physicochemical traits (Tables 2, 3). Therefore, the synergistic effects are not only due to pseudocapacitive contributions induced by chemical aspects but also physical ones by ensuring limited agglomerations and generation of porous channels. The impact of physical attributes is in providing a larger electroactive surface from electrochemical processes, particularly for the EDLC mechanism.

The flexibility and buffering effect on swelling of graphene derivatives have also been utilized in polymer-based composites for SSCs (Tables 2, 3).[141–149] The effect of porosity in SSC electrode materials can be rationalized by identifying the influence of pore sizes. A few reports have focused on the pore size effect on charge storage; thus, future studies could aid in filling this gap, particularly in the case of PSCs. Given the current limitations of the nitrogen sorption analysis for surface area determination due to non-one-one mapping with electroactive surface area, modelling could strategically help in this regard. According to some recent studies, micropores in graphene derivatives directly and positively impact energy storage, particularly via PSC,[143] while mesopores and in-plane nanopores promote electrolyte ion/electron transport within the electrode and shorten diffusion path length, respectively.[59] These are interesting primitive deductions which still need more confirmation studies with different materials such as graphene derivatives.

Cellulose derivatives, such as nanofibers,[150,151] nanofibrils,[152] and nanocellulose,[144,153] have enabled super elasticity and super hydrophilicity in graphene derivative-based SSCs for flexible electronic applications (Table 2). This development is welcomed since cellulose is derived from biomass, which is vastly available and renewable, thus adding to sustainability goals for future SSCs. Cellulose nanofibril-RGO composite pasted on Cu foil using Ag paste displayed a high C_s of 312 F m^{-2} at 30 A m^{-2} and C_s retention of 82% after 5 × 10^3 cycles in PVA-H_2SO_4 (Tabe 2).[152] A different study on cellulose nanofiber-RGO films dipped in PVA-KOH then physically assembled achieved an inferior C_s 250 F cm^{-3} (193 F g^{-1}) at 1 A g^{-1} but higher C_s retention of 94% after 5 × 10^3 cycles (Tabel 2).[150] While differences could be due to the SSC fabrication methods and dissimilar GPEs used, the impact of dimensional and morphological variations between nanofibrils (lower surface area, shorter, and less elongated) and nanofibers (larger surface area to volume ratio, longer, and thinner) cannot be ignored. A similar rationale can be deduced for nanocellulose reviewed in the current work with C_s of 117 F g^{-1} at 0.3 A g^{-1} and C_s retention of 83% after 10^4 cycles (Table 2).[153] Nevertheless, the commendable cycle stability and deterioration could also be additionally influenced by the high oxygen content of GO relative to RGO and the N- and F-doping. A further attempt to improve the performance of cellulose nanofiber-RGO in SSCs using conducting polymers was not fruitful. The ternary composite of PPY-cellulose nanofiber-RGO SSC made by gentle pressing of the electrode and nanofiber hydrogels together attained an even lower C_s retention and C_s of 87% and 196 F g^{-1} at 0.1 mA g^{-1}, respectively (Table 2).[151] Though still scarce, nanoscale cellulose composites with graphene derivatives were only reported in symmetric SSCs in recent times (Tables 2, 3). Given the ease of modifications of cellulose through alcoholic reactions,[154] more use of cellulose as a future research pathway will aid the generation of flexible novel materials for SSCs.

To sum up, composites with transition metals and polymers are the most promising approach for graphene derivative applications in symmetric SSCs (Table 2). This is deduced from the highest C_s for graphene, GO, and RGO, which were 2520 F m^{-2} at 30 A m^{-2} (for MoSSe-graphene-graphitic petal)[108]; 1492 F g^{-1} at 2.5 A g^{-1} (for AC-GO-TiO_2-Zn),[131] and 180 × 10^6 F m^{-3} at 0.5 A m^{-2} (for Co_3O_4-polydopamine-RGO)[148] for symmetric SSCs, respectively. Similarly, the highest E_s for graphene, GO, and RGO were 0.15 kW h kg^{-1} (for Nb_9VO_{25}-histidine-serine-B-graphene quantum dots),[123] 0.01 kW h kg^{-1} (for AC-GO-TiO_2-Zn),[131] and 12 kW h m^{-3} (for Co_3O_4-polydopamine-RGO)[148] for

symmetric SSCs, respectively. This means that future symmetric SSC designs could take advantage of the preliminary evaluations from this review, showing that metal oxide-polymer-graphene derivative ternary composites are the best performers in this regard. Comparatively, RGO is the most studied graphene derivative for symmetric SSCs and most likely this is due to its stable cycle stability and better conductivity traits. To mention a few studies from the reviewed works done with 10^4 cycles, C_s drop of 21%,[155] 2%,[156] 2%,[74] and 0%[46] for RGO, PET-RGO, PEDOT-RGO-MoS_2, and Fe^{3+}-$Ti_3C_2T_x$-S-, N-RGO, respectively, were reported (Table 2). These reports highlight the benefit of synergism on cycle stability induced by compositing. In addition to the C_s and E_s deductions, recent reports suggest that N-doping of graphene derivatives in transition metal-polymer-graphene derivative ternary composites holds great potential as a future research direction for SSCs. Fundamentally, variations in performance are inclined to a widespread of parameters which may reduce the accuracy of comparisons between separate studies. Turning to ML, as a preliminary step in future research, is a potential route to a breakthrough.

Similarly to symmetric SSCs, applications of graphene in asymmetric SSCs are low (Table 3).[10,61,64,70,104,124,125] The Ni-Co LDH-Co_3O_4//graphene asymmetric SSC device cast by blade coating recorded C_s, E_s, and C_s retention of 286 F g^{-1} at 1 A g^{-1}, 67 W h kg^{-1} and 91% after 1.05 × 10^4 cycles (Table 3).[70] This performance was more progressive when compared to graphene in symmetric SSCs (Table 2). However, only one recent pristine graphene study for asymmetric SSC was obtained, thus, it is insufficient for a satisfactory comparison. Besides, the superb performance of graphene in symmetric SSC could be due to the Co-based anode. The asphalt-graphene QDs-NiCo LDH//AC SSC demonstrated high C_s, E_s, and P_s of 360 F g^{-1} at 1 A g^{-1}, 113 W h kg^{-1} and 751 W kg^{-1}, respectively.[125] This study highlighted the significant potential of the under-explored graphene QDs for SSCs. Another outstanding study was with the Ni-MnO_2-CNTs-N-graphene//CNTs-N-graphene SSCs with wider operational temperature and voltage windows of − 20–70 °C and 2.4 V in PVA-$LiClO_4$, respectively, and recorded C_s and E_s of 90 × 10^6 F m^{-3} at 10 A m^{-2} and 79 × 10^3 W h m^{-3} attributed chiefly to a higher packaging density.[64] Interestingly, recent derivatization of graphene for asymmetric SSCs mostly involved Co oxide as composites and recorded high C_s retentions after 10^4 cycles (Table 3 and Figure 7b).[10,61,124,125] The highest C_s was achieved with the asphalt-graphene QDs-NiCo LDH//AC device (360 F g^{-1} at 1 A g^{-1})[125]; however, the P_s was lower than when graphene was applied in symmetric SSCs (Tables 2, 3). There is no clear explanation from recent literature why graphene composites mostly involve Co. Deductions of a proper rationale are also hindered by the low numbers of graphene studies in this area.

For reviewed GO-based asymmetric SSC electrodes,[117,162–165] spin-coated ZnO nanowire-GO//FTO remarkably achieved the highest C_s and retention of 2200 F g^{-1} at 0.03 A g^{-1} and 100% after 5 × 10^3 cycles, respectively[117] (Table 3). A different study of drop cast ZnO nanowire-GO//FTO SSC also attained 100% C_s retention after 3 × 10^4 cycles (Table 3).[165] Although the ZnO nanowire-RGO//FTO studied under the same conditions showed a 60% and 30% decline in C_s and C_s retention in PVA-LiCl relative to GO-based electrodes,[117] other recent studies involving RGO in different electrolytes have generally achieved better performance in terms of C_s, E_s, and P_s in asymmetric SSCs than GO and graphene (Table 3).[140,166–173] This conclusion could be obscured due to the limited availability of recent reports involving GO and graphene using the same PVA-based electrolytes for SSCs relative to RGO (Table 3). On the other hand, more studies involving RGO for SSCs are motivated by its superiority. Therefore, more future studies are recommended for more insights in this regard since the Zn nanowire example (Table 3) suggests the existence of other factors influencing energy storage performances different from conductivity metrics. Furthermore, ML could illuminate this area better and provide a solid basis without wastage of resources. The highest C_s, from the reviewed works, was 4390 F m^{-2} at 3 A m^{-2} for the $CuCo_2O_4$-RGO//Ni-RGO SSCs fabricated by molding and curing for ∼ one month (Table 3).[171] Interestingly, this study revealed the suitability of RGO in both the cathode and anode of a single asymmetric device. Using Zn electrodes as an example in Table 3,[117,165,172,173] it is clear that the morphology and state of the transition metal utilized in composites with RGO are significant performance factors. Therefore, future studies must critically consider proven morphologies, such as nanowires, and oxide forms of metals in SSCs to generate novel materials.

In the reviewed works, graphene derivative applications in SSCs enhanced cycle stability with a minimum and maximum C_s drop of 1% and 39% and 0% and 30% for symmetric and asymmetric designs, respectively (Tables 2, 3). Relative to the graphene derivative applications in symmetric SSC counterparts, their applications in asymmetric SSCs produce devices with better C_s retention after large charge/discharge cycles (Tables 2, 3). Most reported flexible SSCs are symmetric and, thus, have an inferior E_s to their symmetric counterparts. This is because of the lower operational window of the symmetric SSCs.[42]

4.1. Fabrication Methods Overview

Graphene derivatives are synthesized by either a bottom-up or a top-down method. The top-down method involves micromechanical cleavage of graphite to graphene employing a *"sticky tape"* or liquid-phase exfoliation via GO as an intermediate.[9] GO synthesis methods are wide-ranging comprising *chlorate* and *permanganate* methods.[17] The most common approaches in recent times are *permanganate* methods in the form of modified Hummers' and Tour's methods which involve H_2SO_4 and $NaNO_3$, and a combination of H_2SO_4 and H_3PO_4, respectively as additional oxidants to permanganate. There are a variety of versions of methods in literature which seek to tailor physicochemical properties for target applications. Key considerations are experimental conditions and the physicochemical nature of parent materials. Readers are referred to a recent review, by Mombeshora et al.[17] for further details on graphene derivative synthesis.

In the contemporary, RGO and doped species for SSCs are mostly synthesized through hydrothermal/solvothermal routes. This is because the methods are facile, scalable with the right

solvent selection, utilize low temperatures, produce uniform products as reagents are exposed to even conditions and have no greenhouse gas emissions due to a closed autoclave. However, the major drawback is the safety risk if reagents generate excessive internal pressure greater than what can be contained within the autoclave during heating. Other less common reduction methods include sonochemical means in reductants such as L-ascorbic acid[53] and thermal approach.[130] This sonochemical method advantageously uses less material under environmentally friendly conditions of temperatures, pressures, and no waste gas emissions to achieve sheet separation and reduction simultaneously, thus, it is less tedious and has short reaction times. However, the reported achievement of N-doping through ultrasonic protocols in relevant N-containing solvents is debatable. The debate emanates from the less intense energy inputs used against the often-required High energy to force N into substituting C in the graphene framework. The notion here is that thorough characterization of N species is necessary to distinguish surface functionalities from dopants. The bottom-up methods for SSCs are in situ growth of graphene derivatives from elemental carbon on a relevant substrate such as carbon paper or Ni using the plasma-enhanced chemical vapor deposition method.[108] In brief, this path involves pyrolysis of a hydrocarbon followed by nucleation and growth on a substrate. Hence, providing materials with better adhesion to the substrate. However, the deposition of other impurities during synthesis might negate the device's performance. The purification steps that selectively remove carbonaceous impurities are not easy to devise. Also, the bottom-up method has high greenhouse gas emissions that pollute the environment, often involves high temperatures which need a longer duration to cool down, requires high capital investment, and is relatively costly compared to the top-down approach. Nevertheless, the merits are the scalability, facile porosity, and dimensional control.

The graphene-based electrodes for SSCs, particularly for the top-down, are fabricated mostly via the blade coating of active material slurry onto a current collector such as Ni foam[53] and graphite paper[179] (Tables 2, 3). In the fabrication protocol, small amounts of conductive carbon black and binder are added to the active material during the slurry preparation. The effect of binders is often detrimental to the SSC performance but necessary for improved electrical contacts. Therefore, only a sufficient amount needs to be added and if possible, must be avoided. Blade coating is followed by drying and determination of the active material mass. Proper drying is necessary for correct active mass and ultimately accurate C_s values. Recent developments in this area also include in situ derivatization, such as reduction and N-doping, on current collectors using hydrothermal or solvothermal methods (Tables 2, 3).[104] This method allows control of the dimensions of graphene derivatives and is scalable.[28] Another way is pressing the active material onto the current collector foam.[105] In this method excessive compacting must be avoided as it will increase electrolyte penetration resistance by minimizing porosity in the SSC device, thus, lowering energy storage. Spin coating[117] and drop casting[165] of active material onto appropriate current collectors is also feasible. Spin coating poses difficulties in morphology control and is wasteful, posing economic drawbacks. In the pristine graphene application in SSCs, laser engraving[109] is gaining momentum from suitable graphene precursors such as polyamide. The engraving approach allows the development of *2D* electrode materials involving graphene derivatives and promotes the availability of large surface areas in composites involving transition metals. However, carbonization and firing steps in this method can be energy intensive as they use temperatures above 1000 and ~3000 °C, respectively. Recently, the *3D* permeating assemblies that provide electron transport pathways have been reported through *3D* printing of pristine graphene ink in SSCs using temperatures as low as 40 °C 95]. The *3D* printing approach has high precision through programmable layer-by-layer manufacturing steps and allows the fabrication of diverse configurations.[180] In summary, more tailor-made synthesis methods of graphene derivatives for SSCs that offer facile and economic advantages against conventional SCs and batteries are needed to support the drive towards commercialization.

4.2. Charge Storage Mechanism Perceptions

Graphene derivatives, by a large electrode/electrolyte contact area store energy through the EDLC mechanism particularly in symmetric SSCs (Figure 7a).[88] In addition, when applied in asymmetric SSCs, graphene derivatives can function in redox activities. For instance, using PVA-KOH, the oxidative redox process is:

$$RGO + 2OH^- \rightleftharpoons RGO - OH + 2e^- \quad (3)$$

$$GO + 2OH^- \rightleftharpoons GO - OH + 2e^- \quad (4)$$

As anodes of SSCs, graphene derivatives are oxidized (forward reaction of Equations 3,4) and reduced during charging and discharging, respectively,[181] and vice versa when applied as cathodes. However, in most recent designs, particularly for asymmetric SSCs (Table 3), anode is made of a transition metal composite of graphene derivatives. Hence, an additional pseudocapacitive mechanism is:

$$M \rightleftharpoons M^{n+} + ne^- \quad (5)$$

The hopping mechanism is also feasible when GPE electrolytes are used in SSCs. In this mechanism, the rate of formation and breaking of H-bonds between H_3O^+ and the H_2O molecules influences the rate of H^+ transfer.[88] The energy can also be stored through the diffusion of an H^+-H_2O complex and this mechanism is hindered by the formation of H-bonds with other H_2O molecules.[88] A direct transfer of H^+ can also be facilitated via the amorphous phase of the polymer backbone through segmental movements that occur above the glass transition temperature.[88] A similar mechanism can be extrapolated for GPE involving other group one cations (Tables 2, 3). For redox-active solid polymer electrolytes, the pseudocapacitive mechanism occurs through electron transfer between the graphene derivative electrode and electrolyte.[28]

Molecular dynamic simulations and the first-principal inputs of GO and RGO with 17 and 0 wt% oxygen content

established H_2O molecules under an electric field facilitate energy storage.[26] This is attained through charge separations between GO sheets and a distribution parallel to sheets due to polarized water molecules. Since high oxygen content enhances hydrophilicity and in most cases is trapped between sheets. This theoretically suggests that GO has better energy storage capabilities than RGO through this mechanism. This is mostly not the case since simulations are based on ideal models and vary from real-world scenarios. Furthermore, SSCs involving properly dried electrodes will eliminate contributions from trapped water. To sum up, the functions of graphene derivatives in SSCs have been demonstrated. Finally, a summary of their current status and future research directions that can be taken is provided to highlight feasibility, limitations, solutions, and merits.

5. Outlook and Perspective for Graphene Derivatives and SSC Nexus

Practical challenges, merits, advances, and views for future research directions of graphene derivatives for SSC are discussed in this section.

5.1. Challenges and Recommendations for Practical Applications

Although the development of SSCs is regarded as a positive step towards sustainability in renewable energy resources, they are still greatly inferior to liquid electrolyte-based SCs (commonly $< 50\%$ C_s). This means more work is still required to close the gap and make SSCs commercially viable. Two fundamental issues need to be experimentally clarified in future works, that is., establishing whether the inferiority of SSCs is due to design changes or limitations of the solid-state electrolyte. Systematic studies that seek to optimize solid-state electrolytes for specific designs followed by comparison under similar experimental setups are possible solutions to this problem. Currently, the potential of graphene derivatives in solid-state electrolytes is underexplored. However, the few available reports suggest that excessive amounts of graphene derivatives in the solid-state electrolyte deteriorate the SSCs. Since graphene derivatives, except for GO, are appreciably conductive, the most probable rationale for poor performance is charge transport disruptions from high agglomerations at high content. Therefore, modifications of current electrolytes with graphene derivatives can be further explored by considering H-bonds as a future research direction. This is suggested in the drive to improve tolerance of high-temperature issues since most graphene derivatives contain numerous oxygen-containing moieties and can be doped with nitrogen. Chemical linkages through H-bonding can also potentially solve agglomeration issues when only sufficient amounts for bonding are added through optimization, thus, improving component intimacy for better charge transport.

Relative to GO-based materials, superior electronic conducting attributes of RGO-based derivatives bring better performances as electrodes. This brings a technical glitch since on the one hand a high content of oxygen moieties allows facile electrode fabrication with minimum defects due to aggregation. A thorough figure-of-merit that accounts for diversity in the graphene family of materials and the influence of oxygen moieties on performance and processability is suggested. Another challenge associated with adopting graphene derivatives in SSCs is the inconsistent pore size distributions and morphologies which vary with the synthesis method.[17,39] This dictates a need for developing specific chemical compositions of graphene derivatives and tailoring protocols that offer more room for improving electronic properties for SSC applications. In the drive towards flexible electrode materials, it may seem obvious that carbon cloth is the best candidate for flexibility qualities among the other carbon-based materials. However, the costs involved, hydrophobicity nature, and low electro-active surface areas hinder their preference.[182] This underlines the need for affordable alternatives, hence, graphene derivatives, that can tactfully support the accessibility of renewable energy through effective energy storage are recommended. The common self-discharge problems in SSCs still require practical solutions,[29] especially using graphene derivatives since they have high electron conductivity.

5.2. Current Practical Advances of SSCs with Graphene Derivatives

While optimization of synergistic factors induced by current collectors, electrolytes, and electrode materials remains a critical aspect in all forms of SCs,[183] one emerging and promising proven concept[117,165,184,185] is to develop photo-assisted SSCs from graphene derivatives. Photo-assisted SSCs practically allow direct harnessing of sunlight from the sun into storable electrical energy. For example, photo-assisted ZnO nanowire-GO//FTO[165] and FTO/ZnO-RGO/PVA-LiCl/carbon paper[184] SSCs began to function after a few min, supported digital clocks for > 2 h under outdoor sunlight exposure. Hence, this technology potentially has positive prospects in complementing solar energy. This technology requires two fundamental qualities, that is., high transparency to allow efficient energy harnessing and effective energy storage. This is supported by the optical transparency achievable with well-exfoliated graphene derivatives. To illustrate this, Jiang et al.[186] developed MXene quantum dot-laser RGO composites with high transparency ($> 90\%$), high cycle stability (98% after 12000 cycles) and capacitance of 10 mF cm^{-2}. Another emerging technology is the thermally charged SSC in which a temperature change generates a voltage difference to allow energy storage.[28,187] The charging and discharging processes involve absorbing and releasing heat, respectively. This approach is inappropriate for graphene derivatives due to their temperature sensitivity. Their framework is denatured at $\sim$500 °C in air and oxygen moieties are removed in the 200 – 400 °C range. Therefore, RGO and N-RGO under inert environments are highly recommended for thermally charged SSCs.

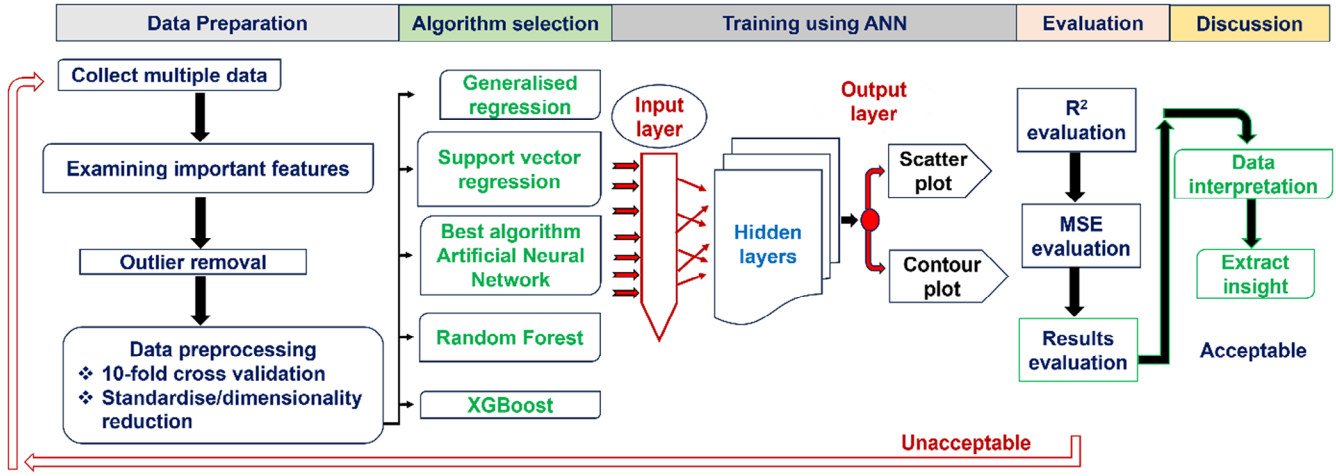

Figure 8. Scheme for ML model generation and validation.

Except for a few studies that use AC instead,[10,61] the current asymmetric SSC design commonly utilizes graphene derivatives as the cathode (Figure 7b). Therefore, this implies that most of the current developments of graphene derivatives are inclined toward modifying the cathodic performance. Reviewed works (Tables 2, 3) suggest that a biased focus on their cathodic role is not satisfactorily justified since numerous highly performing graphene derivative-based anodes for SSCs exist. Though more work is still required to achieve devices with improved flexibility and electrochemical performance, the current modification of SSCs with graphene derivatives has encouraging outcomes. More work is currently focusing on the facile modification of graphene for better electronic properties. Common modifications being sought are surface chemical functionalization, doping, and compositing. The derivatization of graphene has shown several positive prospects. These include improving solution processability via enhanced hydrophilicity, electroactive surface areas from appropriate exfoliation brought by oxygen moieties, better affordability particularly when derived from biomass and expanding operational voltage window. This, in turn, enhances the E_s of SCs. Combining graphene derivatives with other electrode material that functions in a different potential window is a possible step to expand their operational voltage window. Other than only deriving the GO from biomass for SSC applications, some studies have used biomass-derived reductants, such as lemon and carrot juice (C/O ratio increased from 2.5 to ~ 5 and 4, respectively).[188] This illustrates advancements that make graphene derivatives sustainable and transform the energy sector towards "*greener*" characteristics. Furthermore, binder-free SSCs involving graphene derivatives are also emerging.[174] One typical approach is layer-by-layer fabrication through recent techniques such as *3D* printing. These approaches make them more affordable and minimize dead mass and any negative effects of binders on device performance. Therefore, the resulting SSCs have better performance induced by mitigated agglomeration, random orientation with vastly wrinkled sheets, atomistic perforations, and engineered microporosity structure, which support the free movement of electrolyte ions.[189]

5.3. Viewpoint for Machine Learning

In the recent drive towards ML of complex phenomena, ML is being applied in graphene-related materials for SCs. ML uses artificial intelligent function-fitting algorithms trained from some experimental data to learn the underlying relationship between data input and output to develop a model that can predict outcomes for new datasets (Figure 8).[190,191] In SSCs, ML models can use electrochemical measurements and physicochemical traits to predict C_s. Therefore, the physicochemical characteristics of graphene derivatives that can be used in ML of SSCs as inputs for data processing include atomic weight % (wt.%) of carbon and dopants (e.g., boron, oxygen, sulfur, and nitrogen); defect band to graphitic band intensity ratio from Raman spectroscopy; specific surface area, pore size, and volume.[190–192] For synthesis and material tailoring purposes, ML can be used to predict physicochemical properties such as defects in graphene derivatives.[193]

On the other hand, electrochemical characteristics that can be utilized are electrolyte characteristics namely composition, dimensions, and conductivity; SSC configuration; operational conditions such as potential window, current density, scan speed, and method of analysis, charge transfer, and ESR as inputs in the data preparation stage.[23,194,195]

In the preparation stage, numerous literature data will need to be converted from categorical to numerical data through hot encoding for compatibility reasons and randomly grouped into training and test sets (Figure 8). The training set is scaled from 0 (min) to 1 (max) range to minimize complex calculations and the same scale is applied to the validation set. Examining important features of the data is critical but leads to some limitations, for instance, if aqueous electrochemical measurements are considered then the operational voltage window for specific data points will be restricted to < 1 V.[191] Furthermore, if the specific surface area of graphene derivatives is utilized, then the pore structure effects are lost yet they influence C_s. In addition, EDLC is regarded as the major contributor to C_s when specific surface area is considered but this may not be the case for most composites and doped species of

graphene derivatives in which PSC contributions are significant. The challenges of ML applications are that some reports may lack required data inputs and require a vast amount of representative database to generate an accurately trained model. Since the output parameters are C_s, P_s, and E_s, this stage is followed by an analysis of the link between inputs and outputs using supervised ML models (Algorithm selection in Figure 8). In this way, ML has prospects in speeding up the design and optimization of SSC processes by aiding understanding of electrode, electrolyte, and electrode/electrolyte interface processes, thereby minimizing wastage of resources during random trials.

The artificial neural network (ANN) is among the most applied models in predicting C_s of SCs because of its accuracy predictability, capability to deduce underlying mechanisms of complicated systems, generalizability, and compatibility with non-linear data. ANN has multiple variances that aim at linking inputs with hidden layers and involves systematic adjustment to lower statistical biases and weight effects toward an accurate output (Figure 8).[194] ANN requires known numerical values for comparison during training and after sufficient training cycles, it can predict energy storage outputs. For instance, ANN predicted that oxygen and nitrogen content was inversely and directly proportional to C_s in graphene derivatives, respectively.[191] This agrees with most literature reports that suggest that GO is inferior to RGO and N-doped counterparts particularly pyridinic, which adds energy storage via a pseudocapacitive mechanism and is highly conductive. Also, Mahmoudi–Qashqay et al.[194] achieved C_s predictions within ~6% error margin and with a high degree of correlation (R-squared (R^2) = 0.999) for Co_3O_4-VS_4-RGO-based electrodes. Other models, such as the light gradient boost machine, extreme gradient boost, and random forest models are comparable to ANN in predicting C_s of graphene derivatives.[196,197] The performance of each model is checked through the processes highlighted in Figure 8.

The models are then cross validated to check their performance followed by comparing them. The model validations are commonly done using mean square error (MSE), root mean square error (RMSE), mean absolute error (MAE), and R^2 parameters against actual experimental data (Figure 8).[198] Thus, there is a need to standardize SSC characterization protocols to support ML growth. In addition, the widespread physicochemical characteristics of graphene derivatives may bring large standard deviations in the data. Saad et al.[190] minimized the widespread effect by treating each graphene derivative material as a separate class. Other useful references for future development include ML applications for predicting the synergism of hetero atom doping of graphene using the Shapley additive explanation (SHAP).[191,192] SHAP analysis is used to investigate the contributions of each input to the target output through scatter and contour plots, and inputs are then ranked according to impact on output parameters. A positive and negative SHAP value implies positive and negative contributions to C_s, respectively.[190,191] This interesting path will rationalize most references to the synergistic effect made in the literature.

ML relies heavily on the data from which it was trained and improper interpretations lead to failure in capturing physical mechanisms.[191] Hence, to some degree, ML may be limited to established technologies and does not account for the underlying physics of SSCs as each input is considered in a numerical value form. ML modelling is still scarce in SSCs and the most probable reasons are linked to the fact that graphene derivative-based SSCs are still emerging. In brief, this review proposes that future research focuses on this area. This will pave the way for accelerated development of novel SSC designs. Given the interlinking of contributing factors to C_s, ML will simplify technological and scientific problems and provide fast-track solutions. Furthermore, ML will allow the development of tailoring protocols from graphene derivative synthesis steps to SSC devices. In this regard, ML will significantly aid the rationalization of compounding effects of physicochemical properties of graphene derivatives, solid-state electrolytes, SSC fabrication method, test conditions such as current density and scan speed and SSC test methods on C_s, E_s, and P_s.

5.4. Future Research Directions, Prospects, and Conclusions

Future research directions should include a focus on developing novel solid-state electrolytes that not only exhibit high ionic conductivity,[55,199] but also, high flexibility. Improving flexibility attributes through graphene derivatives will positively support the growing demand for wearable and smart electronics and a wider operational temperature range as future advancements. The fabrication of flexible SSCs is still in its infancy and reviewed recent works suggest that the most commonly applied solid-state electrolyte is the GPE (Tables 2, 3). This could be rationalized by their superior conductivity relative to dry-solid polymer electrolytes.[63] Considering the superb operational voltage window of up to 6 V,[55] one prospective game changer is the development of solvent-free ionic liquid gel electrolytes in combination with graphene derivatives. Another lucrative future approach is the integration of graphene derivatives with solid-sate electrolytes in *3D* configurations to maximize electrode/electrolyte interface contact. Additionally, since solid-state electrolytes are essential in the future provision of mechanically stable, durable, and temperature-resistant SCs, this supports the notion that current developments involving graphene derivatives in SSCs represent a positive step towards enhanced durability. Long-term stability is possible by achieving wider operational temperature ranges, thus ensuring minimal freezing that maintains high ionic conductivity and reduces decomposition at lower and higher temperatures.

Developments of new SSC designs and standardized optimization studies can also illuminate the design aspect needed for E_s improvements. In this regard, nano- and micro-sized SSCs are research directions with promising traits for current energy storage needs. Several general design pathways, such as coaxial, interwoven, typographic, twisted, knitted, and lithographic techniques,[30,200] are suitable prospects for SSC. However, most configurations were for pristine graphene and are still primitive for practical graphene derivative applications. To date, hybridization of graphene derivatives with pseudo-capacitive materials and doping of graphene derivatives seem to have high potential

to improve E_s, whilst maintaining high P_s. Therefore, synthesizing novel materials for electrodes and electrolytes becomes a foundational aspect of SSC transformation in the next few years. This motivates a future focus on graphene derivatives in both electrodes and electrolytes of SSCs. This basis should also acknowledge and factor in the impact of the synthesis method of graphene derivatives as this contributes to the overall performance of the materials in SSCs.[17,143]

Future research approaches must further explore the combination of graphene derivatives with ultrathin *2D* pseudocapacitive layered materials, such as reported $Co(OH)_2$ nanosheets,[110] chalcogenides,[55] Mxenes,[201] and borophene[129] as electrodes for flexible SSCs. On the one hand, these materials will add favorable energy storage functionalities to graphene derivatives. For instance, Mxenes are layered structures of carbides, nitrides of transition metals, and carbon with high electrical conductivity, interlayer diffusion pathways and electroactive area for energy storage function.[87,201] Layered *2D* materials theoretically possess an enhanced electroactive area with valence electrons for better electrode/electrolyte interactions,[202] thus, they are promising in future SSCs. However, the electrolyte ion penetration is reduced by invertible agglomeration during SSC fabrication.[203] On the other hand, the shortfalls of *2D* materials can also be modified with graphene derivatives, such as N-doped graphene, given the noted improvements when they are used. The graphene derivatives can also play a role in maximizing the available electroactive area by minimizing layers from collapsing onto each other in *2D* materials. Therefore, this potential approach can advance novel materials and SSC flexible designs as a future research direction. The derivatization of graphene minimizes dead mass by promoting the exfoliation of sheet and engineering porosity. Thus, it is a practical step in enhancing electrochemical properties for SSC development.

Positive attributes of SSCs involving graphene derivatives in real-world applications include a wider operational voltage window, for instance, PVA-Na_2SO_4 polymer electrolytes have recorded an operational voltage window as high as 2.0 V and attenuation rates of 48% within a self-discharge period of a day.[99] This highlights the significant potential of graphene derivatives in enhancing the E_s of SSCs. The commonly reported approach for composites of graphene derivatives in SSCs encompasses conductive enhancers and separators to reduce aggregation. High intimacy between graphene derivatives and additives via chemical linkages in typical materials has achieved commendable performances in SSCs. A fundamental morphological approach involving graphene derivative composites will transform materials into a *3D* graphene sheet that can offer more surfaces for energy storage.

To sum up, the key areas that still require further research in SSCs include the study of the role and performance impacts of graphene derivatives in electrolytes, and performance improvements, particularly E_s, against the conventional liquid electrolyte-based SCs. Comparative studies of PVA-group one sulfates with GO- and RGO-based electrodes are recommended as future research directions to enable better comparisons in SSCs. A better way to mitigate the lack of standardized testing protocols is to compare electrolytes in one study. The *3D* morphology engineering using other emerging *2D* materials and graphene QDs for SSCs is also an attractive area for further studies. Investigating the compatibility of graphene derivatives in both flexible and photo-assisted devices, end-of-life analysis and environmental impact of graphene derivative-based SSCs, and recycling options are also areas that still need more work. Concerning long-term stability tests, more studies under controlled harsh environments of humidity, moisture, temperature, and light irradiation are critical to enlighten their practical applicability. This will give insights into the areas for suitable SSC applications that can emanate from these materials. The SCs generally lack a standardized testing protocol that would make comparisons between researchers and materials easy. Therefore, ML modelling is a proposed future solution to determine quantifiable relationships among critical factors of graphene derivative-based SSC electrodes and their impacts. Graphene-based SSC electrodes offer more room for achieving environmental sustainability through cost-effective biomass sources. However, indirect harm to the environment from the use of toxic chemicals, such as N_2H_4, H_2SO_4, and H_3PO_4, that are harmful to aquatic life and carcinogenic to humankind, and emission of greenhouse gases, such as NO_x and CO_x, during material synthesis must be monitored carefully and avoided where possible. In addition, recycling protocols similar to batteries can be applied to graphene derivative-based SSCs. These involve mechanical separation, thermal treatment, and mechanochemical treatments. Chemical means, such as acid leaching and purification through a dissolution process of other components, are also feasible recycling steps. These feasibilities make graphene derivative-based SSCs attractive for future innovations. In addition, graphene-based SSC electrodes allow porosity, electroconductivity, redox activity, stability tailoring, and widening of operational voltage window. Hence, highly performing electrode materials for SSCs are feasible with graphene derivatives since tailoring their electronic structures and physicochemical properties makes it easy to achieve the prerequisites. Therefore, graphene derivatives in SSCs can effectively support the power dynamics required for the internet of everything. The use of graphene derivatives, particularly RGO, is promising for future state-of-the-art SSCs that need to meet current demands for flexibility, safety in handling, portability, long cycle life, and mechanical robustness in advanced electronics. The future of technologically advanced electronics such as biomedical equipment, wearable electronics, and microsensors will benefit hugely from the SSC developments.

Acknowledgements

This work was supported by the Faculty of Engineering and the Built Environment, University of the Witwatersrand. The authors acknowledge the University of the Witwatersrand and Bindura University of Science Education for supporting this work and providing the necessary research infrastructure.

Conflict of Interests

The authors declare no conflict of interest.

Data Availability Statement

Data sharing is not applicable to this article as no new data was created or analyzed in this study.

Keywords: Electrochemical capacitor · Energy storage · Gel electrolytes · Graphene · Machine learning

[1] J.-H. Lee, G. Yang, C.-H. Kim, R. L. Mahajan, S.-Y. Lee, S.-J. Park, *Energy Environ. Sci.* **2022**, *15*, 2233–2258, https://doi.org/10.1039/d1ee03567c.
[2] R. Ghanbari, S. R. Ghorbani, *J. Energy Storage* **2023**, *60*, 106670, https://doi.org/10.1016/j.est.2023.106670.
[3] D. J. Patil, D. B. Malavekar, J. H. Kim, C. D. Lokhande, *J. Energy Storage* **2023**, *72*, 108729, https://doi.org/10.1016/j.est.2023.108729.
[4] A. Arya, M. Iqbal, S. Tanwar, A. Sharma, A. L. Sharma, V. Kumar, *Mater. Sci. Eng. B* **2022**, *285*, 115972, https://doi.org/10.1016/j.mseb.2022.115972.
[5] M. Jalalah, S. S. Sivasubramaniam, B. Aljafari, M. Irfan, S. S. Almasabi, T. Alsuwian, M. I. Khazi, A. K. Nayak, F. A. Harraz, *J. Energy Storage* **2022**, *54*, 105210, https://doi.org/10.1016/j.est.2022.105210.
[6] E. T. Mombeshora, P. G. Ndungu, A. L. L. Jarvis, V. O. Nyamori, *Int. J. Energy Res.* **2017**, *41*, 1182–1201, https://doi.org/10.1002/er.3702.
[7] R. Mendoza, M. Balderas-Soto, R. G. Suarez, J. Zamora, A. I. Mtz-Enriquez, A. Zakhidov, J. Oliva, *Synth. Met.* **2024**, *306*, 117654, https://doi.org/10.1016/j.synthmet.2024.117654.
[8] H. Yu, J. G. Kim, D. M. Lee, S. Lee, M. G. Han, J. W. Park, S. M. Kim, N. D. Kim, H. S. Jeong, *Adv. Energy Mater.* **2023**, *14*, 2303003, https://doi.org/10.1002/aenm.202303003.
[9] E. T. Mombeshora, A. Stark, *Biomass Convers. Biorefin.* **2023**, *13*, 4619–4638, https://doi.org/10.1007/s13399-021-01499-6.
[10] H. Guo, A. Zhang, H. Fu, H. Zong, F. Jin, K. Zhao, J. Liu, *Chem. Eng. J.* **2023**, *453*, 139633, https://doi.org/10.1016/j.cej.2022.139633.
[11] M. Saquib Khan, B. SanthiBhushan, K. Chandra Bhamu, S. Gu Kang, H. Singh Kushwaha, A. Sharma, R. Dhiman, R. Gupta, M. Kumar Banerjee, K. Sachdev, *Appl. Surf. Sci.* **2023**, *607*, 154990, https://doi.org/10.1016/j.apsusc.2022.154990.
[12] E. T. Mombeshora, P. G. Ndungu, A. L. L. Jarvis, V. O. Nyamori, *Mater. Chem. Phys.* **2018**, *213*, 102–112, https://doi.org/10.1016/j.matchemphys.2018.03.076.
[13] T. N. Vinuth Raj, P. A. Hoskeri, S. Hamzad, M. S. Anantha, C. M. Joseph, H. B. Muralidhara, K. Y. Kumar, F. A. Alharti, B.-H. Jeon, M. S. Raghu, *Inorg. Chem. Commun.* **2022**, *142*, 109648, https://doi.org/10.1016/j.inoche.2022.109648.
[14] M. Li, B. Xu, L. Zheng, J. Zhou, Z. Luo, W. Li, W. Ma, Q. Mao, H. Xiang, M. Zhu, *Carbon* **2023**, *203*, 455–461, https://doi.org/10.1016/j.carbon.2022.11.102.
[15] A. Viswanathan, V. Aravindan, *RSC Sustainability* **2024**, *2*, 2199–2212, https://doi.org/10.1039/d4su00133h.
[16] D. Dhamodharan, P. P. Ghoderao, V. Dhinakaran, S. Mubarak, N. Divakaran, H.-S. Byun, *J. Ind. Eng. Chem.***2022**, *106*, 20–36, https://doi.org/10.1016/j.jiec.2021.10.033.
[17] E. T. Mombeshora, E. Muchuweni, *RSC Advances* **2023**, *13*, 17633-17655, https://doi.org/10.1039/d3ra02098c.
[18] J. R. Xavier, R. B. J., *J. Alloys Compd.* **2023**, *947*, 169483, https://doi.org/10.1016/j.jallcom.2023.169483.
[19] S. Tamang, S. Rai, R. Bhujel, N. K. Bhattacharyya, B. P. Swain, J. Biswas, *J. Alloys Compd.* **2023**, *947*, 169588, https://doi.org/10.1016/j.jallcom.2023.169588.
[20] E. Muchuweni, E. T. Mombeshora, C. M. Muiva, T. S. Sathiaraj, *J. Energy Storage* **2023**, *73*, 109013, https://doi.org/10.1016/j.est.2023.109013.
[21] S. Yasa, O. Kumbasi, M. B. Arvas, M. Gencten, M. Sahin, Y. Sahin, *ECS J. Solid State Sci. Technol.* **2023**, *12*, 051002, https://doi.org/10.1149/2162-8777/acd3af.
[22] A. Jain, S. R. Manippady, R. Tang, H. Nishihara, K. Sobczak, V. Matejka, M. Michalska, *Sci. Rep.* **2022**, *12*, 21024, https://doi.org/10.1038/s41598-022-25707-z.
[23] S. Nanda, S. Ghosh, T. Thomas, *J. Power Sources* **2022**, *546*, 231975, https://doi.org/10.1016/j.jpowsour.2022.231975.
[24] S. Sardana, K. Aggarwal, S. Malik, A. Saini, S. Dahiya, R. Punia, A. S. Maan, K. Singh, A. Ohlan, *Electrochim. Acta* **2022**, *434*, 141324, https://doi.org/10.1016/j.electacta.2022.141324.
[25] M. Zhang, D. Jiang, F. Jin, Y. Sun, J. Wang, M. Jiang, J. Cao, B. Zhang, J. Liu, *J. Colloid Interface Sci.* **2023**, *636*, 204–215, https://doi.org/10.1016/j.jcis.2022.12.159.
[26] Y. Gao, Y. Wan, B. Wei, Z. Xia, *Adv. Funct. Mater.* **2018**, *28*, 1706721, https://doi.org/10.1002/adfm.201706721.
[27] V. Kumaravel, J. Bartlett, S. C. Pillai, *Adv. Energy Mater.* **2020**, *11*, 2002869, https://doi.org/10.1002/aenm.202002869.
[28] M. Akin, X. Zhou, *Int. J. Energy Res.* **2022**, *46*, 10389-10452, https://doi.org/10.1002/er.7918.
[29] S. S. Patil, T. S. Bhat, A. M. Teli, S. A. Beknalkar, S. B. Dhavale, M. M. Faras, M. M. Karanjkar, P. S. Patil, *Eng. Sci.* **2020**, *12*, 38–51, https://doi.org/10.30919/es8d1140.
[30] M. K. Jha, C. Subramaniam, *ACS Omega* **2021**, *6*, 7970–7978, https://doi.org/10.1021/acsomega.1c00172.
[31] M. S. Asl, R. Hadi, L. Salehghadimi, A. G. Tabrizi, S. Farhoudian, A. Babapoor, M. Pahlevani, *J. Energy Storage* **2022**, *50*, 104223, https://doi.org/10.1016/j.est.2022.104223.
[32] Y. H. Song, T. Kim, U. H. Choi, *Chem. Mater.* **2020**, *32*, 3879–3892, https://doi.org/10.1021/acs.chemmater.0c00041.
[33] T. Lv, M. Liu, D. Zhu, L. Gan, T. Chen, *Adv. Mater.* **2018**, *30*, e1705489, https://doi.org/10.1002/adma.201705489.
[34] L. Lv, B. Hui, X. Zhang, Y. Zou, D. Yang, *Chem. Eng. J.* **2023**, *452*, 139443, https://doi.org/10.1016/j.cej.2022.139443.
[35] E. T. Mombeshora, V. O. Nyamori, *Int. J. Energy Res.* **2015**, *39*, 1955–1980, https://doi.org/10.1002/er.3423.
[36] Y. Sim, S. Surendran, H. Cha, H. Choi, M. Je, S. Yoo, D. Chan Seok, Y. Ho Jung, C. Jeon, D. Jin Kim, M.-K. Han, H. Choi, U. Sim, J. Moon, *Chem. Eng. J.* **2022**, *428*, 132086, https://doi.org/10.1016/j.cej.2021.132086.
[37] A. Agrawal, A. Kumar, A. Gaur, *J. Energy Storage* **2022**, *56*, 105990, https://doi.org/10.1016/j.est.2022.105990.
[38] W. Chen, C. Hao, Z. Qiu, X. Zhang, H. Xu, B. Yu, S. Chen, *ACS Appl. Mater. Interfaces* **2022**, *14*, 19534-19546, https://doi.org/10.1021/acsami.2c02507.
[39] S. Ratha, S. Sahoo, P. Mane, B. Polai, B. Sathpathy, B. Chakraborty, S. K. Nayak, *Sci. Rep.* **2023**, *13*, 5283, https://doi.org/10.1038/s41598-022-23574-2.
[40] J. Zhao, J. Zhang, H. Yin, Y. Zhao, G. Xu, J. Yuan, X. Mo, J. Tang, F. Wang, *Nanomaterials* **2022**, *12*, 1210, https://doi.org/10.3390/nano12071210.
[41] S. Pappu, S. Anandan, T. N. Rao, S. K. Martha, S. V. Bulusu, *J. Energy Storage* **2022**, *50*, 104598, https://doi.org/10.1016/j.est.2022.104598.
[42] D. M. Sayed, N. K. Allam, *J. Energy Storage* **2022**, *56*, 105882, https://doi.org/10.1016/j.est.2022.105882.
[43] E. T. Mombeshora, E. Muchuweni, M. L. Davies, V. O. Nyamori, B. S. Martincigh, in Handbook of Emerging Materials for Sustainable Materials for Energy, (Eds.: N. V. Kulkarni, B. I. Kharissov), Elsevier, Oxford, England, UK **2024**, pp. 83–118, https://doi.org/10.1016/C2021-0-02074-5.
[44] M. Ates, O. Yoruk, Y. Bayrak, M. Turkyilmaz, H. Karabulut, *Ionics* **2024**, *30*, 5391–5410, https://doi.org/10.1007/s11581-024-05684-1.
[45] E. T. Mombeshora, E. Muchuweni, M. L. Davies, V. O. Nyamori, B. S. Martincigh, *Energy sci. eng.* **2022**, *10*, 3493–3506, https://doi.org/10.1002/ese3.1234.
[46] X. Yang, M. Zhang, C. Wang, M. Bi, J. Xie, W. Bai, Y. Zhang, S. Pan, M. Liu, X. Pan, Z. Lu, Z. Han, Y. Fu, *J. Energy Storage* **2023**, *71*, 108140, https://doi.org/10.1016/j.est.2023.108140.
[47] P. Bhojane, P. M. Shirage, *J. Energy Storage* **2022**, *55*, 105649, https://doi.org/10.1016/j.est.2022.105649.
[48] S. Rahimpour, E. Payami, L. Luo, R. Teimuri-Mofrad, *J. Organomet. Chem.* **2024**, 123240, https://doi.org/10.1016/j.jorganchem.2024.123240.
[49] U. V. Gopi, P. Bhojane, K. S. Smaran, *J. Energy Storage* **2022**, *54*, 105301, https://doi.org/10.1016/j.est.2022.105301.
[50] V. M. Maphiri, D. T. Bakhoum, S. Sarr, N. F. Sylla, G. Rutavi, N. Manyala, *J. Energy Storage* **2022**, *52*, 104967, https://doi.org/10.1016/j.est.2022.104967.
[51] W. Yan, Y. Zhang, T. Zeng, Y. Zhang, Q. Wan, N. Yang, *J. Energy Storage* **2022**, *52*, 104899, https://doi.org/10.1016/j.est.2022.104899.

[52] E. S. Goda, S. E. Hong, B. Pandit, A. ur Rehman, B. S. Singu, M. S. Akhtar, M. Sohail, S. M. El-Bahy, H. Gamal, K. R. Yoon, *J. Alloys Compd.* **2023**, *965*, 171183, https://doi.org/10.1016/j.jallcom.2023.171183.
[53] A. Paul, S. Ghosh, H. Kolya, C.-W. Kang, N. Chandra Murmu, T. Kuila, *Chem. Eng. J.* **2022**, *443*, 136453, https://doi.org/10.1016/j.cej.2022.136453.
[54] D.-L. Lu, R.-R. Zhao, J.-L. Wu, J.-M. Ma, M.-L. Huang, Y.-B. Yao, T. Tao, B. Liang, J.-W. Zhai, S.-G. Lu, *J. Eur. Ceram. Soc.* **2020**, *40*, 2396–2403, https://doi.org/10.1016/j.jeurceramsoc.2020.02.006.
[55] Y. Yang, T. Zhu, L. Shen, Y. Liu, D. Zhang, B. Zheng, K. Gong, J. Zheng, X. Gong, *SmartMat* **2022**, *3*, 349–383, https://doi.org/10.1002/smm2.1103.
[56] E. T. Mombeshora, E. Muchuweni, M. L. Davies, B. S. Martincigh, V. O. Nyamori, *New J. Chem.* **2023**, *47*, 3502–3515, https://doi.org/10.1039/d2nj05112eDoi:10.1039/d2nj05112e.
[57] B. Huang, J. Yuan, Y. Lu, Y. Zhao, X. Qian, H. Xu, G. He, H. Chen, *Chem. Eng. J.* **2022**, *436*, 135231, https://doi.org/10.1016/j.cej.2022.135231.
[58] S. Rudra, N. Deka, A. K. Nayak, M. Pradhan, G. K. Dutta, *J. Energy Storage* **2022**, *50*, 104615, https://doi.org/10.1016/j.est.2022.104615.
[59] C. Jiang, M. Gao, S. Zhang, L. Huang, S. Yu, Z. Song, Q. Wu, *Int. J. Biol. Macromol.* **2023**, *225*, 1437–1448, https://doi.org/10.1016/j.ijbiomac.2022.11.201.
[60] G. Zhou, G. Liang, W. Xiao, L. Tian, Y. Zhang, R. Hu, Y. Wang, *Molecules* **2024**, *29*, 1262, https://doi.org/10.3390/molecules29061262.
[61] H. Ansarinejad, M. Shabani-Nooshabadi, S. M. Ghoreishi, *J. Energy Storage* **2022**, *45*, 103513, https://doi.org/10.1016/j.est.2021.103513.
[62] A. Mendhe, H. S. Panda, *Discover Materials* **2023**, *3*, 29, https://doi.org/10.1007/s43939-023-00065-3.
[63] S. Samantaray, D. Mohanty, I. M. Hung, M. Moniruzzaman, S. K. Satpathy, *J. Energy Storage* **2023**, *72*, 108352, https://doi.org/10.1016/j.est.2023.108352.
[64] K. Qin, J. Baucom, L. Diao, Y. Lu, N. Zhao, *Small* **2022**, *18*, e2203166, https://doi.org/10.1002/smll.202203166.
[65] S. M. Youssry, M. A. Elkodous, R. Kumar, G. Kawamura, W. K. Tan, A. Matsuda, *Electrochim. Acta* **2023**, *463*, 142814, https://doi.org/10.1016/j.electacta.2023.142814.
[66] B. Liu, Q. Zhang, L. Zhang, C. Xu, Z. Pan, Q. Zhou, W. Zhou, J. Wang, L. Gu, H. Liu, *Adv. Mater.* **2022**, *34*, e2106309, https://doi.org/10.1002/adma.202106309.
[67] N. Kamboj, R. S. Dey, *Electrochim. Acta* **2022**, *421*, 140499, https://doi.org/10.1016/j.electacta.2022.140499.
[68] D. Sahoo, J. Shakya, S. Choudhury, S. S. Roy, L. Devi, B. Singh, S. Ghosh, B. Kaviraj, *ACS Omega* **2022**, *7*, 16895-16905, https://doi.org/10.1021/acsomega.1c06852.
[69] Y. K. Sonia, S. K. Meher, *Energy Fuels* **2023**, *37*, 4010–4025, https://doi.org/10.1021/acs.energyfuels.2c03467.
[70] A. G. El-Deen, M. K. Abdel-Sattar, N. K. Allam, *Appl. Surf. Sci.* **2022**, *587*, 152548, https://doi.org/10.1016/j.apsusc.2022.152548.
[71] Z. Lu, X. Liu, T. Wang, X. Huang, J. Dou, D. Wu, J. Yu, S. Wu, X. Chen, *J. Colloid Interface Sci.***2023**, *638*, 709–718, https://doi.org/10.1016/j.jcis.2023.02.013.
[72] K. Sun, S. Cui, X. Gao, X. Liu, T. Lu, H. Wei, H. Peng, G. Ma, *J. Energy Storage* **2023**, *61*, 106658, https://doi.org/10.1016/j.est.2023.106658.
[73] B. Asbani, C. Douard, T. Brousse, J. Le Bideau, *Energy Storage Mater.* **2019**, *21*, 439–445, https://doi.org/10.1016/j.ensm.2019.06.004.
[74] A. Bagheri, S. Bellani, H. Beydaghi, M. Eredia, L. Najafi, G. Bianca, M. I. Zappia, M. Safarpour, M. Najafi, E. Mantero, Z. Sofer, G. Hou, V. Pellegrini, X. Feng, F. Bonaccorso, *ACS Nano* **2022**, *16*, 16426-16442, https://doi.org/10.1021/acsnano.2c05640.
[75] P. Wang, Y. Zhang, H. Jiang, X. Dong, C. Meng, *Chem. Eng. J.* **2022**, *427*, 131548, https://doi.org/10.1016/j.cej.2021.131548.
[76] K. Nasrin, S. Gokulnath, M. Karnan, K. Subramani, M. Sathish, *Energy Fuels* **2021**, *35*, 6465–6482, https://doi.org/10.1021/acs.energyfuels.1c00341.
[77] S. Krishnan, A. K. Gupta, M. K. Singh, N. Guha, D. K. Rai, *Chem. Eng. J.* **2022**, *435*, 135042, https://doi.org/10.1016/j.cej.2022.135042.
[78] N. An, W. Li, Z. Shao, L. Zhou, Y. He, D. Sun, X. Dong, Z. Hu, *J. Energy Storage* **2023**, *57*, 106180, https://doi.org/10.1016/j.est.2022.106180.
[79] A. Amiri, A. Bruno, A. A. Polycarpou, *Carbon Energy* **2023**, *5*, e320, https://doi.org/10.1002/cey2.320.
[80] M. M. Amaral, R. Venâncio, A. C. Peterlevitz, H. Zanin, *J. Energy Chem.* **2022**, *67*, 697–717, https://doi.org/10.1016/j.jechem.2021.11.010.
[81] X. Hu, Y. Chen, Z. Hu, Y. Li, Z. Ling, *J. Electrochem. Soc.* **2018**, *165*, A1269–A1274, https://doi.org/10.1149/2.0481807jes.
[82] B. Pandit, S. R. Rondiya, R. W. Cross, N. Y. Dzade, B. R. Sankapal, *Chem. Eng. J.* **2022**, *429*, 132505, https://doi.org/10.1016/j.cej.2021.132505.
[83] K. Zhang, Y. Pang, C. Chen, M. Wu, Y. Liu, S. Yu, L. Li, Z. Ji, J. Pang, *Carbohydr. Polym.*, **2022**, *293*, 119673, https://doi.org/10.1016/j.carbpol.2022.119673.
[84] M. Shi, W. Yang, Z. Zhang, M. Zhao, Z. L. Wang, X. Lu, *J. Mater. Chem. A* **2022**, *10*, 2966–2972, https://doi.org/10.1039/d1ta08709f.
[85] E. T. Mombeshora, R. Simoyi, V. O. Nyamori, P. G. Ndungu, *S. Afr. J. Chem.* **2015**, *68*, 153–164, https://doi.org/10.17159/0379-4350/2015/v68a22.
[86] S. Hong, H. Kim, S. Gao, R. L. Lavall, H. Y. Jung, Y. J. Jung, *J. Power Sources* **2019**, *432*, 16–23, https://doi.org/10.1016/j.jpowsour.2019.05.065.
[87] J. Peng, M. Zhou, Y. Gao, J. Wang, Y. Cao, W. Wang, D. Wu, Y. Yang, *J. Mater. Chem. A* **2021**, *925*, 25073–25085, https://doi.org/10.1039/d1ta06617j.
[88] S. Alipoori, S. Mazinani, S. H. Aboutalebi, F. Sharif, *J. Energy Storage* **2020**, *27*, 101072, https://doi.org/10.1016/j.est.2019.101072.
[89] M. Shoeb, F. Mashkoor, M. Naved Khan, B.-J. Kim, C. Jeong, *Sep. Purif. Technol.* **2025**, *354*, 128656, https://doi.org/10.1016/j.seppur.2024.128656.
[90] T. E. Somesh, Siddaramaiah, T. Demappa, *J. Solid State Chem.* **2022**, *309*, 122824, https://doi.org/10.1016/j.jssc.2021.122824.
[91] Y. Zhang, C.-g. Zhou, X.-h. Yan, Y. Cao, H.-l. Gao, H.-w. Luo, K.-z. Gao, S.-c. Xue, X. Jing, *J. Power Sources* **2023**, *565*, 232916, https://doi.org/10.1016/j.jpowsour.2023.232916.
[92] P. Mehra, A. Paul, *J. Phys. Chem. C* **2022**, *126*, 6135–6146, https://doi.org/10.1021/acs.jpcc.1c10829.
[93] S. Majumdar, P. Sen, R. Ray, *J. Solid State Electrochem.* **2022**, *26*, 527–547, https://doi.org/10.1007/s10008-021-05093-8.
[94] W.-C. Lai, R.-W. Fan, *J. Electroanal. Chem.* **2022**, *907*, 115889, https://doi.org/10.1016/j.jelechem.2021.115889.
[95] J. Shen, Y. Dai, F. Xia, X. Zhang, *Sustainable Mater. Technol.* **2023**, *36*, e00586, https://doi.org/10.1016/j.susmat.2023.e00586.
[96] Z. Li, C. Ji, F. Guo, H. Mi, X. Zhu, J. Qiu, *J. Mater. Chem. A* **2022**, *10*, 4671–4682, https://doi.org/10.1039/d1ta10138b.
[97] S. Majumdar, P. Sen, R. Ray, *Mater. Res. Bull.* **2022**, *151*, 111814, https://www.sciencedirect.com/science/article/pii/S0025540822000885.
[98] D. Lei, Q. Zhang, N. Liu, Z. Liu, T. Su, L. Wang, Z. Ren, P. Jia, W. Lu, Y. Gao, *Cell Rep. Phys. Sci.***2022**, *3*, 101050, https://doi.org/10.1016/j.xcrp.2022.101050.
[99] H. Jiang, J. Chen, Y. Shi, P. Chen, X. Tang, W. Jiang, Z. Zou, G. Wu, *Appl. Surf. Sci.* **2022**, *586*, 152739, https://doi.org/10.1016/j.apsusc.2022.152739.
[100] T. Chen, T. Shen, Y. Wang, Z. Yu, W. Zhang, Y. Zhang, Z. Ouyang, Q. Cai, Y. Ji, S. Wang, *ACS Omega* **2023**, *8*, 10888-10898, https://doi.org/10.1021/acsomega.2c07187.
[101] S. Dalvand, Z. Khoushab, S. M. Mousavi-Khoshdel, H. Ghafuri, H. R. Esmaili Zand, M. Omidvar, *Int. J. Hydrogen Energy* **2023**, *48*, 10098-10107, https://doi.org/10.1016/j.ijhydene.2022.12.026.
[102] H. S. Tripathi, A. Dutta, T. P. Sinha, *Electrochim. Acta* **2022**, *421*, 140505, https://doi.org/10.1016/j.electacta.2022.140505.
[103] R. Kumar, S. Sahoo, E. Joanni, R. K. Singh, R. M. Yadav, *Mater. Today, Nano.***2023**, *24*, 100399, https://doi.org/10.1016/j.mtnano.2023.100399.
[104] A. Bahaa, M. A. Abdelkareem, H. Al Naqbi, A. Yousef Mohamed, P. A. Shinde, B. A. A. Yousef, E. T. Sayed, H. Alawadhi, K. J. Chae, S. Al-Asheh, A. G. Olabi, *J. Colloid Interface Sci.***2022**, *608*, 711–719, https://doi.org/10.1016/j.jcis.2021.09.136.
[105] B. Zhang, L. Gao, H. Bai, Y. Li, B. Jia, X. Zhou, A. Li, L. Li, *J. Alloys Compd.* **2023**, *934*, 167979, https://doi.org/10.1016/j.jallcom.2022.167979.
[106] M. Vandana, S. Veeresh, H. Ganesh, Y. S. Nagaraju, H. Vijeth, M. Basappa, H. Devendrappa, *J. Energy Storage* **2022**, *46*, 103904, https://doi.org/10.1016/j.est.2021.103904.
[107] N. Chadha, M. Y. Bhat, S. A. Hashmi, P. Saini, *J. Energy Storage* **2022**, *46*, 103789, https://doi.org/10.1016/j.est.2021.103789.
[108] N. K., S. R. Polaki, C. S. Rout, *J. Energy Storage* **2022**, *52*, 105007, https://doi.org/10.1016/j.est.2022.105007.
[109] X. Zhao, D. He, B. You, *Mater. Today, Energy.* **2022**, *17*, 232916, https://doi.org/10.1016/j.mtsust.2021.100096.
[110] P. B. Jagdale, S. A. Patil, M. Pathak, P. Bhol, A. Sfeir, S. Royer, A. K. Samal, C. S. Rout, M. Saxena, *J. Mater. Chem. A* **2024**, *12*, 17350-17359, https://doi.org/10.1039/d4ta02916j.

[111] S. Kumar, M. Goswami, N. Singh, P. Soni, N. Sathish, S. Kumar, *Carbon Lett.* **2022**, *32*, 979–985, https://doi.org/10.1007/s42823-022-00331-z.
[112] K. M. A. Raihan, S. Sahoo, T. Nagaraja, S. Sigdel, B. LaCroix, C. M. Sorensen, S. R. Das, *APL Energy* **2024**, *2*, 016104, https://doi.org/10.1063/5.0186302.
[113] S.-C. Han, J.-L. Quan, F.-G. Zhou, Y.-H. Xue, N. Li, F.-Y. Li, D. Wang, *Rare Met.* **2022**, *42*, 971–981, https://doi.org/10.1007/s12598-022-02202-y.
[114] M. Karbak, O. Boujibar, S. Lahmar, C. Autret-Lambert, T. Chafik, F. Ghamouss, *J. Carbon Res.* **2022**, *8*, 27, https://doi.org/10.3390/c8020027.
[115] F. Mo, H. Zhang, Y. Wang, C. Chen, X. Wu, *J. Energy Storage* **2022**, *49*, 104122, https://doi.org/10.1016/j.est.2022.104122.
[116] L. Wang, X. Ma, D. Chen, J. Zhou, H. Qin, H. Ma, *Small Struct.* **2024**, *5*, 2300329, https://doi.org/10.1002/sstr.202300329.
[117] C. T. Altaf, A. M. Rostas, M. Mihet, M. D. Lazar, I. Iatsunskyi, E. Coy, E. Erdem, M. Sankir, N. D. Sankir, *J. Mater. Chem. C* **2022**, *10*, 10748-10758, https://doi.org/10.1039/d2tc02114e.
[118] N. Wang, G. Zhang, T. Guan, J. Wu, J. Wang, K. Li, *ACS Appl. Mater. Interfaces.***2022**, *14*, 13250-13260, https://doi.org/10.1021/acsami.1c23624.
[119] P. A. Le, V. Q. Le, N. T. Nguyen, V. B. T. Phung, *RSC Advances* **2022**, *12*, 1515–1526, https://doi.org/10.1039/d1ra07820h.
[120] S. Zhu, F. Zhang, H.-G. Lu, J. Sheng, L. Wang, S.-D. Li, G. Han, Y. Li, *ACS Mater. Lett.* **2022**, *4*, 1863–1871, https://doi.org/10.1021/acsmaterialslett.2c00616.
[121] B. Bai, J. Shui, Y. Wang, Z. Su, L. Qiu, P. Du, *ACS Appl. Nano Mater.* **2024**, *7*, 12387-12398, https://doi.org/10.1021/acsanm.4c00494.
[122] E. S. Goda, B. Pandit, S. E. Hong, B. S. Singu, S. K. Kim, E. B. Moustafa, K. R. Yoon, *J. Energy Chem.* **2022**, *74*, 429–445, https://doi.org/10.1016/j.jechem.2022.07.033.
[123] L. Xiaoshan, L. Ruiyi, L. Zaijun, Y. Yongqiang, L. Xiaohao, *J. Ind. Eng. Chem.* **2024**, https://doi.org/10.1016/j.jiec.2024.06.036.
[124] E. S. Goda, A. ur Rehman, B. Pandit, A. Al-Shahat Eissa, S. E. Hong, K. Ro Yoon, *Chem. Eng. J.* **2022**, *428*, 132470, https://doi.org/10.1016/j.cej.2021.132470.
[125] Y. Yan, L. Xie, Y. Zhou, Y. Li, C.-M. Chen, *J. Energy Storage* **2024**, *95*, 112458, https://doi.org/10.1016/j.est.2024.112458.
[126] R. Dadashi, M. Bahram, M. Faraji, *J. Energy Storage* **2022**, *52*, 104775, https://doi.org/10.1016/j.est.2022.104775.
[127] Q. Wang, H. Song, W. Li, S. Wang, L. Liu, T. Li, Y. Han, *J. Power Sources* **2022**, *517*, 230737, https://doi.org/10.1016/j.jpowsour.2021.230737.
[128] B. Antil, L. Kumar, M. R. Das, S. Deka, *J. Energy Storage* **2022**, *52*, 104731, https://doi.org/10.1016/j.est.2022.104731.
[129] O. P. Nanda, C. Y. Kong, S. Badhulika, *ACS Appl. Energy Mater.* **2024**, *7*, 7844–7853, https://doi.org/10.1021/acsaem.4c01437.
[130] E. T. Mombeshora, P. G. Ndungu, V. O. Nyamori, *Electrochim. Acta* **2017**, *258*, 467–476, https://doi.org/10.1016/j.electacta.2017.11.084.
[131] S. Veeresh, H. Ganesha, Y. S. Nagaraju, H. Vijeth, H. Devendrappa, *J. Alloys Compd.* **2023**, *952*, 169907, https://doi.org/10.1016/j.jallcom.2023.169907.
[132] Y. Wang, J. Lu, Y. Zhao, H. Lv, Z. Zhou, H. Wei, Z. Chen, *J. Colloid Interface Sci.***2022**, *609*, 114–129, https://doi.org/10.1016/j.jcis.2021.11.128.
[133] J. Dong, Y. Zhou, H. Du, Y. Li, Y. Wanga, Z. Qin, Polyaniline nanorod array grown on graphene oxide through in–situ **2024**, SSRN: https://ssrn.com/abstract?=?4873802, https://doi.org/10.2139/ssrn.4873802.
[134] C. Liang, L. Zang, F. Shi, C. Yang, J. Qiu, Q. Liu, Z. Chen, *Cellulose* **2022**, *29*, 2525–2537, https://doi.org/10.1007/s10570-022-04454-4.
[135] T. Guan, Z. Cheng, Z. Li, L. Gao, K. Yan, L. Shen, N. Bao, *Ind. Eng. Chem. Res.* **2022**, *61*, 3840–3849, https://doi.org/10.1021/acs.iecr.2c00067.
[136] J. Wang, Y. Huang, Y. Gao, J. Dai, X. Sun, *J. Energy Storage* **2022**, *51*, 104581, https://doi.org/10.1016/j.est.2022.104581.
[137] D. Scarpa, M. Iuliano, C. Cirillo, P. Iovane, C. Borriello, S. Portofino, E. Ponticorvo, S. Galvagno, M. Sarno, *Sci. Rep.* **2024**, *14*, 14998, https://doi.org/10.1038/s41598-024-65635-8.
[138] S. Wang, Y. Li, Q. Xu, Q. Fu, X. Guo, Y. Zheng, W. Zhang, Z. Cao, R. Li, J. Ren, *Nanoscale* **2022**, *14*, 15908-15917, https://doi.org/10.1039/d2nr04723c.
[139] M. Chen, X. Yu, H. Huang, J. Ji, L. Li, *Adv. Mater. Technol.* **2024**, *9*, 2400297, https://doi.org/10.1002/admt.202400297.
[140] A. Mohammadi Zardkhoshoui, B. Ameri, S. Saeed Hosseiny Davarani, *Chem. Eng. J.* **2023**, *470*, 144132, https://doi.org/10.1016/j.cej.2023.144132.
[141] E. T. Mombeshora, E. Muchuweni, *Discover Materials* **2023**, *3*, 32, https://doi.org/10.1007/s43939-023-00068-0.
[142] W. Teng, Q. Zhou, G. Lv, P. Hu, Y. Du, H. Li, Y. Hu, W. Liu, J. Wang, *J. Colloid Interface Sci.***2023**, *636*, 245–254, https://doi.org/10.1016/j.jcis.2023.01.019.
[143] S. Gadipelli, J. Guo, Z. Li, C. A. Howard, Y. Liang, H. Zhang, P. R. Shearing, D. J. L. Brett, *Small Methods* **2023**, *7*, e2201557, https://doi.org/10.1002/smtd.202201557.
[144] H. Liu, T. Xu, C. Cai, K. Liu, W. Liu, M. Zhang, H. Du, C. Si, K. Zhang, *Adv. Funct. Mater.* **2022**, *32*, 2113082, https://doi.org/10.1002/adfm.202113082.
[145] Y. He, X. Ning, L. Wan, *Polym. Bull.* **2021**, *79*, 9075–9091, https://doi.org/10.1007/s00289-021-03948-8.
[146] V. Molahalli, V. S. Bhat, A. Shetty, D. Hundekal, A. Toghan, G. Hegde, *J. Energy Storage* **2023**, *69*, 107953, https://doi.org/10.1016/j.est.2023.107953.
[147] Y. Yu, A. Xu, Y. Zhang, Z. Zhao, S. Ye, Y. Qin, *Electrochim. Acta* **2023**, *454*, 142414, https://doi.org/10.1016/j.electacta.2023.142414.
[148] A. Bouzina, R. Meng, F. Pillier, H. Perrot, C. Debiemme-Chouvy, O. Sel, *J. Mater. Chem. A* **2024**, *12*, 17688-17701, https://doi.org/10.1039/d4ta02392g.
[149] S. Ye, A. Xu, W. Cao, Z. Zhao, S. Zhang, Y. Qin, *Langmuir* **2024**, *40*, 11460-11469, https://doi.org/10.1021/acs.langmuir.4c00316.
[150] H. Wu, W. Yuan, X. Yuan, L. Cheng, *Carbon Energy* **2022**, *5*, e229, https://doi.org/10.1002/cey2.229.
[151] H. Qiang, W. He, F. Guo, J. Cao, R. Wang, Z. Guo, *ACS Appl. Nano Mater.* **2022**, *5*, 6305–6315, https://doi.org/10.1021/acsanm.2c00397.
[152] H. Liu, T. Xu, Q. Liang, Q. Zhao, D. Zhao, C. Si, *Adv. Compos. Hybrid Mater.* **2022**, *5*, 1168–1179, https://doi.org/10.1007/s42114-022-00427-0.
[153] Y. Zhang, Q. Zhou, W. Ma, C. Wang, X. Wang, J. Chen, T. Yu, S. Fan, *Nano Res.* **2023**, *16*, 9519–9529, https://doi.org/10.1007/s12274-023-5736-5.
[154] E. T. Mombeshora, E. Muchuweni, A. J. Doolin, M. L. Davies, B. S. Martincigh, V. O. Nyamori, *Appl. Mater. Today* **2024**, *40*, 102406, https://doi.org/10.1016/j.apmt.2024.102406.
[155] K. S. Perera, K. P. Vidanapathirana, L. J. Adams, C. S. Hawes, N. Balakrishnan, *J. Energy Storage* **2024**, *97*, 112683, https://doi.org/10.1016/j.est.2024.112683.
[156] X. Chen, M. Gu, *Ultrafast Sci.* **2022**, *2022*, 0001, https://doi.org/10.34133/ultrafastscience.0001.
[157] Z. Wang, S. Yao, S. Wang, Z. Liu, X. Wan, Q. Hu, Y. Zhao, C. Xiong, L. Li, *Chem. Eng. J.* **2023**, *463*, 142427, https://doi.org/10.1016/j.cej.2023.142427.
[158] A. R. Thiruppathi, J. van der Zalm, L. Zeng, M. Salverda, P. C. Wood, A. Chen, *J. Energy Storage* **2022**, *48*, 103962, https://doi.org/10.1016/j.est.2022.103962.
[159] R. Sankannavar, R. Bhosale, R. Kangutkar, S. Kolekar, J. Manjanna, *J. Energy Storage* **2024**, *94*, 112455, https://doi.org/10.1016/j.est.2024.112455.
[160] Y. Zhao, F. Liu, Z. Zhao, P. Bai, Y. Ma, A. Alhadhrami, G. A. M. Mersal, Z. Lin, M. M. Ibrahim, Z. M. El-Bahy, *Adv. Compos. Hybrd. Mater.***2022**, *5*, 1516–1526, https://doi.org/10.1007/s42114-022-00488-1.
[161] W. Li, A. Xu, Y. Zhang, Y. Yu, Z. Liu, Y. Qin, *J. Alloys Compd.* **2022**, *897*, 162640, https://doi.org/10.1016/j.jallcom.2021.162640.
[162] S. V. Sadavar, N. S. Padalkar, R. B. Shinde, A. S. Patil, U. M. Patil, V. V. Magdum, Y. M. Chitare, S. P. Kulkarni, R. N. Bulakhe, V. G. Parale, J. L. Gunjakar, *ACS Appl. Energy Mater.* **2022**, *5*, 2083–2095, https://doi.org/10.1021/acsaem.1c03619.
[163] M. B. Poudel, H. J. Kim, *J. Energy Chem.* **2022**, *64*, 475–484, https://doi.org/10.1016/j.jechem.2021.05.002.
[164] X. Wu, F. Zeng, X. Song, X. Sha, H. Zhou, X. Zhang, Z. Liu, M. Yu, C. Jiang, *Chem. Eng. J.* **2023**, *456*, 140947, https://doi.org/10.1016/j.cej.2022.140947.
[165] C. T. Altaf, T. O. Colak, A. M. Rostas, M. Mihet, M. D. Lazar, I. Iatsunskyi, E. Coy, I. D. Yildirim, F. B. Misirlioglu, E. Erdem, M. Sankir, N. D. Sankir, *J. Energy Storage* **2023**, *68*, 107694, https://doi.org/10.1016/j.est.2023.107694.
[166] S. J. Marje, V. V. Patil, V. G. Parale, H.-H. Park, P. A. Shinde, J. L. Gunjakar, C. D. Lokhande, U. M. Patil, *Chem. Eng. J.* **2022**, *429*, 132184, https://doi.org/10.1016/j.cej.2021.132184.
[167] C. Jagtap, V. Kadam, B. Kamble, P. E. Lokhande, A. Pakdel, D. Kumar, R. Udayabhaskar, A. Vedpathak, N. B. Chaure, H. M. Pathan, *J. Energy Storage* **2024**, *83*, 110666, https://doi.org/10.1016/j.est.2024.110666.
[168] P. A. K. Reddy, H. Han, K. C. Kim, S. Bae, *Chem. Eng. J.* **2023**, *471*, 144608, https://doi.org/10.1016/j.cej.2023.144608.
[169] S. Harini, V. Anto Feradrick Samson, J. Fennyl Britto, A. Sherin Steena, J. Madhavan, M. Victor Antony Raj, *Emergent Mater.* **2024**, https://doi.org/10.1007/s42247-024-00776-0.

[170] K. Nasrin, M. Arunkumar, N. K. Kumar, V. Sudharshan, S. Rajasekar, D. Mukhilan, M. Arshad, M. Sathish, *Chem. Eng. J.* **2023**, *474*, 145505, https://doi.org/10.1016/j.cej.2023.145505.
[171] C. Fang, D. Zhang, *Electrochim. Acta* **2022**, *401*, 139491, https://doi.org/10.1016/j.electacta.2021.139491.
[172] J.-J. Yao, C. Liu, J.-Y. Li, Z.-L. Hu, R.-Y. Zhou, C.-C. Guo, X.-R. Liu, F.-F. Yang, Y.-R. Zhu, *Rare Met.* **2023**, *42*, 2307–2323, https://doi.org/10.1007/s12598-023-02265-5.
[173] Y. Deng, H. Wang, K. Zhang, J. Qiu, L. Yan, *Adv. Sustainable Syst.* **2021**, *6*, 2100191, https://doi.org/10.1002/adsu.202100191.
[174] P. K. Katkar, S. A. Patil, J. H. Jeon, H. R. Na, N. S. Padalkar, S.-K. Jerng, S. Lee, S.-H. Chun, *Energy Fuels* **2022**, *36*, 13356-13369, https://doi.org/10.1021/acs.energyfuels.2c02875.
[175] W. Liu, X. Zhang, Y. Xu, L. Wang, Z. Li, C. Li, K. Wang, X. Sun, Y. An, Z. S. Wu, Y. Ma, *Adv. Funct. Mater.* **2022**, *32*, 2202342, https://doi.org/10.1002/adfm.202202342.
[176] R. S. Karmur, D. Gogoi, S. Sharma, M. R. Das, A. Dalvi, N. N. Ghosh, *J. Mater. Chem. A* **2024**, *12*, 12762-12776, https://doi.org/10.1039/d4ta01042f.
[177] N. S. Padalkar, S. V. Sadavar, R. B. Shinde, A. S. Patil, U. M. Patil, V. V. Magdum, Y. M. Chitare, S. P. Kulkarni, R. N. Bulakhe, V. G. Parale, J. L. Gunjakar, *Electrochim. Acta* **2022**, *424*, 140615, https://doi.org/10.1016/j.electacta.2022.140615.
[178] H. Zong, A. Zhang, J. Dong, Y. He, H. Fu, H. Guo, F. Liu, J. Xu, J. Liu, *Chem. Eng. J.* **2023**, *475*, 146088, https://doi.org/10.1016/j.cej.2023.146088.
[179] J. Liu, Z. Khanam, S. Ahmed, H. Wang, T. Wang, S. Song, *J. Power Sources* **2021**, *488*, 229461, https://doi.org/10.1016/j.jpowsour.2021.229461.
[180] X. Tian, B. Xu, *Small Methods* **2021**, *5*, e2100877, https://doi.org/10.1002/smtd.202100877.
[181] V. Shanmugapriya, G. Hariharan, B. Selvakumar, S. Bharathi, A. Arivarasan, *Diamond Relat. Mater.* **2024**, *148*, 111505, https://doi.org/10.1016/j.diamond.2024.111505.
[182] T. Kshetri, D. D. Khumujam, T. I. Singh, Y. S. Lee, N. H. Kim, J. H. Lee, *Chem. Eng. J.* **2022**, *437*, 135338, https://doi.org/10.1016/j.cej.2022.135338.
[183] J. Salamon, A. Simi, H. J. Prabu, A. Felix Sahayaraj, A. J. S. Kennedy, V. Snowlin, R. R. Gopi, I. Johnson, *Polym. Compos.* **2024**, *45*, 12899-12912, https://doi.org/10.1002/pc.28676.
[184] C. T. Altaf, T. O. Colak, A. M. Rostas, C. Socaci, M. D. Lazar, L. B. Tudoran, M. H. Aleinawi, F. B. Misirlioglu, I. D. Yildirim, E. Erdem, N. D. Sankir, M. Sankir, *Energy Adv.* **2024**, *3*, 1965–1976, https://doi.org/10.1039/D4YA00253A.
[185] A. Das Mahapatra, S. Kumar, P. S. Chauhan, A. Mondal, A. Sutradhar, A. Misra, *ACS Appl. Energy Mater.* **2024**, *7*, 5801–5810, https://doi.org/10.1021/acsaem.4c00902.
[186] Y. Yuan, L. Jiang, X. Li, P. Zuo, X. Zhang, Y. Lian, Y. Ma, M. Liang, Y. Zhao, L. Qu, *Adv. Mater.* **2022**, *34*, e2110013, https://doi.org/10.1002/adma.202110013.
[187] Q. Wang, P. Liu, F. Zhou, L. Gao, D. Sun, Y. Meng, X. Wang, *Molecules* **2022**, *27*, 1239, https://doi.org/10.3390/molecules27041239.
[188] R. Joshi, A. De Adhikari, A. Dey, I. Lahiri, *Mater. Sci. Eng., B* **2023**, *287*, 116128, https://doi.org/10.1016/j.mseb.2022.116128.
[189] S. Vinothini, A. K. Keyan, S. Sakthinathan, T.-W. Chiu, N. Vittayakorn, *Inorganics* **2024**, *12*, 164, https://doi.org/10.3390/inorganics12060164.
[190] A. G. Saad, A. Emad-Eldeen, W. Z. Tawfik, A. G. El-Deen, *J. Energy Storage* **2022**, *55*, 105411, https://doi.org/10.1016/j.est.2022.105411.
[191] A. Chenwittayakhachon, K. Jitapunkul, B. Nakpalad, P. Worrayotkovit, S. Namuangruk, P. Sirisinudomkit, P. Iamprasertkun, *2D Materials* **2023**, *10*, 025003, https://doi.org/10.1088/2053-1583/acaf8d.
[192] K. Deshsorn, K. Payakkachon, T. Chaisrithong, K. Jitapunkul, L. Lawtrakul, P. Iamprasertkun, *J. Chem. Inf. Model.* **2023**, *63*, 5077–5088, https://doi.org/10.1021/acs.jcim.3c00670.
[193] B. Zheng, Z. Zheng, G. X. Gu, *Nanomaterials (Basel)* **2021**, *11*, 2341, https://doi.org/10.3390/nano11092341.
[194] S. Mahmoudi-Qashqay, M.-R. Zamani-Meymian, A. Maleki, Z. Z. Lahrami, *J. Power Sources* **2024**, *613*, 234911, https://doi.org/10.1016/j.jpowsour.2024.234911.
[195] Q. A. Sial, U. Safder, S. Iqbal, R. B. Ali, *Sustainability* **2024**, *16*, 1516, https://doi.org/10.3390/su16041516.
[196] N. Kati, F. Ucar, *Fractal and Fractional* **2023**, *7*, 218, https://doi.org/10.3390/fractalfract7030218.
[197] R. Dubey, V. Guruviah, *Ionics* **2022**, *28*, 2169–2183, https://doi.org/10.1007/s11581-022-04480-z.
[198] K. Rajguru, S. Bhandari, G. K. Shrestha, C. L. Gnawali, B. P. Pokharel, *BIBECHANA* **2024**, *21*, 159–170, https://doi.org/10.3126/bibechana.v21i2.62465.
[199] Q. Zheng, X. Li, Q. Yang, C. Li, G. Liu, Y. Wang, P. Sun, H. Tian, C. Wang, X. Chen, J. Shao, *J. Power Sources* **2022**, *524*, 231102, https://doi.org/10.1016/j.jpowsour.2022.231102.
[200] D.-Y. Wu, J.-J. Shao, *Mater. Chem. Front.* **2021**, *5*, 557–583, https://doi.org/10.1039/d0qm00291g.
[201] N. Khan, R. Ullah, M. Khan, Almas, *Electrochim. Acta* **2024**, *505*, 144988, https://doi.org/10.1016/j.electacta.2024.144988.
[202] R. Balu, S. K. Sundaram, S. Rameshkumar, K. Aravinth, P. Ramasamy, *J. Electroanal. Chem.* **2022**, *922*, 116718, https://doi.org/10.1016/j.jelechem.2022.116718.
[203] B. Li, M. Yu, Z. Li, C. Yu, H. Wang, Q. Li, *Adv. Funct. Mater.* **2022**, *32*, 2201166, https://doi.org/10.1002/adfm.202201166.

Manuscript received: September 11, 2024